IFN-γ reporter activities at ⩽5 × Cmax in at least 2 of 3 experiments. Digoxin suppressed IL-2 reporter activity at ⩽5 × Cmax in 2 of 3 experiments, while it suppressed IL-2 and IFN-γ reporter activities at >5 × Cmax in 3 experiments. AA augmented IL-2 and IFN-γ reporter activities at ⩽5 × Cmax in 3 experiments and 4 reporter activities at >5 × Cmax. The statistical analysis of the examinations in which only 2 out of 3 experiments demonstrated consistent results showed significant suppression in IL-8 and IL-1β reporter activities by warfarin at ⩽5 × Cmax.

4. Discussion

We developed an immunotoxicity assay system, the Multi-ImmunoTox Assay (MITA), with 3 reporter cell lines that can evaluate the effects of chemicals on the promoter activity of IL-2, IFN-γ, IL-1β, and IL-8. Then, we demonstrated the tight correlation between the evaluation of the effects of 3 representative immunosuppressive drugs based on MITA and that based on mRNA expression of the mother cell lines, Jurkat cells and THP-1 cells. There was a minor discrepancy between the two assays. The assay based on qPCR demonstrated significant augmentation of IL-1β or IL-8 mRNA expression by THP-1 cells treated with CyA or Tac. Although we do not know the exact reason for the discrepancy, the results obtained by HWBCMET suggest that the data obtained by MITA are more appropriate.

Next, we demonstrated the correlation between the evaluation of the effects of these 3 immunosuppressive drugs based on MITA and that based on mRNA expression of whole blood cells. In the originally reported HWBCRA, the final output was determined by the amount of released cytokines. In contrast, our altered method of HWBCRA, HWBCMET, measured mRNA expression of cytokines by qPCR. When we compared the immunosuppressive effects of Dex, CyA, and Tac recognized by HWBCMET with those by the original HWBCRA, which were reported by Langezaal et al. (2002), the qualitative HWBCMET evaluation of these 3 immunosuppressive drugs was consistent with that of HWBCRA. Namely, in both assays, CyA and Tac were more potent in the suppression of T cell cytokine expression than Dex, while Dex was more potent in the suppression of monocyte cytokine expression than CyA and Tac. Next, we demonstrated that the qualitative evaluation of Dex, CyA and Tac was consistent between HWBCMET and MITA, which indicates that the qualitative evaluation by MITA was also consistent with that by the original HWBCRA. Furthermore, the results demonstrating that CyA or Tac significantly suppressed both IL-2 and IFN-γ mRNA induction after stimulation with PMA/Io, while only Dex significantly suppressed IL-1β and IL-8 mRNA induction by LPS, are consistent with the previously reported effects of these drugs on human T cells or macrophages (reviewed in Saag (2008) and Furst and Clements (2008)).

Moreover, in general, when immunotoxicity of chemicals is examined by using human blood cells or murine spleen cells, it is not easy to determine whether the immunotoxicity is caused by their effects on T cells or antigen presenting cells such as monocytes and dendritic cells because of the difficulty in purifying each population. Indeed, HWBCRA cannot confidently determine whether the detected immunological effects of chemicals are due to their direct effects on T cells or antigen presenting cells. In contrast, since MITA uses established T cell and monocyte cell lines, it can separately determine immunotoxicity of chemicals on T cells and monocytes.

In the present study, although we demonstrated that MITA can correctly characterize the effects of 3 representative immunosuppressive drugs, Dex, CyA, and Tac, on the cytokine production by T cells as well as monocytes, it did not reveal the immunosuppressive effects of rapamycin, an alkylating agent or inhibitors of purine or pyrimidine synthesis. Rapamycin inhibits the action of growth-promoting cytokines, while both alkylating agents and antimetabolites induce immunosuppressive effects through their inhibitory action on cell division (reviewed by Hardinger et al. (2004)). In general, immunotoxicity assays detecting the inhibitory effects of chemicals on cytokine expression may not be able to detect their immunosuppressive effects. Indeed, HWBCRA could not detect the immunotoxicity of CP, AZ, and MZR either since the log IC50 values against release of IL-4 by CP, AZA, and MZR were beyond their therapeutic plasma concentrations (Langezaal et al., 2002). The Fluorescent Cell Chip (FCC) could not detect immunotoxicity of cyclophosphamide (Wagner et al., 2006). Therefore, at present, to overcome the drawbacks of these assays, they may need to be combined with assays that can detect the inhibitory action of chemicals on cell division, such as the conventional 28-day subacute toxicity test (Investigators, 1998).

Unexpectedly, rapamycin, CP or inhibitors of purine or pyrimidine synthesis augmented some reporter activities mostly at >5 × Cmax. Since these immunosuppressive drugs inhibit cell growth at much lower concentration than they augment reporter activities, these effects might be overlooked in an *in vivo* system. Further investigation is required to clarify their mechanism and the significance in detecting immunotoxicity *in vitro*.

In addition to AZ and MZR, we also examined immunosuppressive effects of drugs evaluated by HWBCRA, such as colchicine, AA, digoxin, and warfarin (Langezaal et al., 2002). MITA did not detect any suppressive effects of AA on the 4 reporter activities at any concentration. Similarly, the log IC50 values against release of both IL-1β and IL-4 by AA were greater than 1 mM and much higher than 5 × Cmax. MITA detected inhibitory effects of warfarin in IL-1β and IL-8 reporter activities, but not those in IL-2 or IFN-γ reporter activities. Likewise, HWBCRA revealed that warfarin suppressed IL-1β formation more strongly than IL-4 formation. Moreover, MITA demonstrated that digoxin suppressed IL-2 and IFN-γ reporter activities. Similarly, HWBCRA showed that it suppressed IL-4 release. These data are also consistent with the recent publication demonstrating the immunological effects of digoxin (Huh et al., 2011). Therefore, although MITA detected some immunological effects in presumptive non-immunological drugs, these drugs might have unrecognized immunoregulatory activities.

Finally, in the present study, we presented the performance of MITA in evaluation of immunosuppressive or immunostimulatory activities of chemicals and demonstrated that MITA can distinguish which cells, either T cells or monocytes, were primary targets for immunological effects of chemicals. We have already reported that, without any additional stimuli, THP-G8 cells can predict skin sensitizers with test accuracies of greater than 80% (IL-8 Luc assay) (Takahashi et al., 2011). Thus, taking the present and previous studies into consideration, we believe that MITA combined with the IL-8 Luc assay can present a novel high-throughput assay to detect immunotoxicity of chemicals and provide insight into their mechanism in humans. The obtained information from these assays can be used to assess the risks from chemicals by industries as well as regulatory agencies. Needless to say, a larger number of chemicals must be evaluated by MITA to determine the potential and limits of this technique.

Conflict of Interest

The authors declare that there are no conflicts of interest.

Transparency Document

The Transparency document associated with this article can be found in the online version.

Funding

This work was supported in part by a Health and Labor Sciences Research Grant in Japan and by the Ministry of Economy, Trade and Industry.

Appendix A. Supplementary material

Supplementary data associated with this article can be found, in the online version, at http://dx.doi.org/10.1016/j.tiv.2014.02.013.

References

Allison, A.C., 2000. Immunosuppressive drugs: the first 50 years and a glance forward. Immunopharmacology 47, 63–83.

Balls, M., Goldberg, A.M., Fentem, J.H., Broadhead, C.L., Burch, R.L., Festing, M.F., Frazier, J.M., Hendriksen, C.F., Jennings, M., van der Kamp, M.D., Morton, D.B., Rowan, A.N., Russell, C., Russell, W.M., Spielmann, H., Stephens, M.L., Stokes, W.S., Straughan, D.W., Yager, J.D., Zurlo, J., van Zutphen, B.F., 1995. The three Rs: the way forward: the report and recommendations of ECVAM Workshop 11. Altern. Lab. Anim.: ATLA 23, 838–866.

Capell, H.A., Madhok, R., 2008. Disease-modifying antirheumatic drugs 2: sulfasalazine. In: Hochberg, M.C., Silman, A.J., Smolen, J.S., Weinblatt, M.E., Weisman, M.H. (Eds.), Rheumatology (Oxford). fourth ed. Mosby Elsevier, Philadelphia, pp. 437–447.

Chaiamnuay, S., Alarcon, G.S., 2008. Antibiotics. In: Hochberg, M.C., Silman, A.J., Smolen, J.S., Weinblatt, M.E., Weisman, M.H. (Eds.), Rheumtology, fourth ed. Mosby Elsevier, Philadelphia, pp. 433–436.

Furst, D.E., Clements, P.J., 2008. Immunosuppressives. In: Hochberg, M.C., Silman, A.J., Smolen, J.S., Weinblatt, M.E., Weisman, M.H. (Eds.), Rheumatology (Oxford), fourth ed. Mosby Elsevier, Philadelphia, pp. 471–480.

Galbiati, V., Mitjans, M., Corsini, E., 2010. Present and future of in vitro immunotoxicology in drug development. J. Immunotoxicol. 7, 255–267.

Gennari, A., Ban, M., Braun, A., Casati, S., Corsini, E., Dastych, J., Descotes, J., Hartung, T., Hooghe-Peters, R., House, R., Pallardy, M., Pieters, R., Reid, L., Tryphonas, H., Tschirhart, E., Tuschl, H., Vandebriel, R., Gribaldo, L., 2005. The use of in vitro systems for evaluating immunotoxicity: the report and recommendations of an ECVAM workshop. J. Immunotoxicol. 2, 61–83.

Hardinger, K.L., Koch, M.J., Brennan, D.C., 2004. Current and future immunosuppressive strategies in renal transplantation. Pharmacotherapy 24, 1159–1176.

Hartung, T., 2002. Comparison and validation of novel pyrogen tests based on the human fever reaction. Altern. Lab. Anim. : ATLA 30 (Suppl 2), 49–51.

Huh, J.R., Leung, M.W., Huang, P., Ryan, D.A., Krout, M.R., Malapaka, R.R., Chow, J., Manel, N., Ciofani, M., Kim, S.V., Cuesta, A., Santori, F.R., Lafaille, J.J., Xu, H.E., Gin, D.Y., Rastinejad, F., Littman, D.R., 2011. Digoxin and its derivatives suppress TH17 cell differentiation by antagonizing RORgammat activity. Nature 472, 486–490.

Investigators, T.I.G., 1998. Report of validation study of assessment of direct immunotoxicity in the rat. The ICICIS group investigators. International collaborative immunotoxicity study. Toxicology 125, 183–201.

Kiang, T.K., Schmitt, V., Ensom, M.H., Chua, B., Hafeli, U.O., 2012. Therapeutic drug monitoring in interstitial fluid: a feasibility study using a comprehensive panel of drugs. J. Pharm. Sci. 101, 4642–4652.

Langezaal, I., Hoffmann, S., Hartung, T., Coecke, S., 2002. Evaluation and prevalidation of an immunotoxicity test based on human whole-blood cytokine release. Altern. Lab. Anim.: ATLA 30, 581–595.

Lankveld, D.P., Van Loveren, H., Baken, K.A., Vandebriel, R.J., 2010. In vitro testing for direct immunotoxicity: state of the art. Methods Mol. Biol. 598, 401–423.

Livak, K.J., Schmittgen, T.D., 2001. Analysis of relative gene expression data using real-time quantitative PCR and the 2(-Delta Delta C(T)) method. Methods 25, 402–408.

Saag, K., 2008. Systemic glucocorticoids in rheumatology. In: Hochberg, M.C., Silman, A.J., Smolen, J.S., Weinblatt, M.E., Weisman, M.H. (Eds.), Rheumtology, fourth ed. Mosby Elsevier, Philadelphia, pp. 411–419.

Saito, R., Hirakawa, S., Ohara, H., Yasuda, M., Yamazaki, T., Nishii, S., Aiba, S., 2011. Nickel differentially regulates NFAT and NF-kappaB activation in T cell signaling. Toxicol. Appl. Pharmacol. 254, 245–255.

Schindler, S., Hartung, T., 2002. Comparison and validation of novel pyrogen tests based on the human fever reaction. Dev. Biol. (Basel) 111, 181–186.

Sturrock, R.D., 2008. Disease-modifying antirheumatic drugs 1: antimalarials and gold. In: Hochberg, M.C., Silman, A.J., Smolen, J.S., Weinblatt, M.E., Weisman, M.H. (Eds.), Rheumatology (Oxford), fourth ed. Mosby Elsevier, Philadelphia, pp. 433–436.

Surjana, D., Damian, D.L., 2011. Nicotinamide in dermatology and photoprotection. Skinmed 9, 360–365.

Takahashi, T., Kimura, Y., Saito, R., Nakajima, Y., Ohmiya, Y., Yamasaki, K., Aiba, S., 2011. An in vitro test to screen skin sensitizers using a stable THP-1-derived IL-8 reporter cell line, THP-G8. Toxicol. Sci. 124, 359–369.

Thurm, C.W., Halsey, J.F., 2005. Measurement of cytokine production using whole blood. Curr. Protoc. Immunol., Chapter 7, Unit 7 18B.

Wagner, W., Walczak-Drzewiecka, A., Slusarczyk, A., Biecek, P., Rychlewski, L., Dastych, J., 2006. Fluorescent cell chip a new in vitro approach for immunotoxicity screening. Toxicol. Lett. 162, 55–70.

Wiskirchen, D.E., Shepard, A., Kuti, J.L., Nicolau, D.P., 2011. Determination of tissue penetration and pharmacokinetics of linezolid in patients with diabetic foot infections using in vivo microdialysis. Antimicrob. Agents Chemother. 55, 4170–4175.

The Journal of Immunology

Alarmin Function of Cathelicidin Antimicrobial Peptide LL37 through IL-36 γ Induction in Human Epidermal Keratinocytes

Na Li, Kenshi Yamasaki, Rumiko Saito, Sawako Fukushi-Takahashi, Ryoko Shimada-Omori, Masayuki Asano and Setsuya Aiba

J Immunol 2014; 193:5140-5148; Prepublished online 10 October 2014;
doi: 10.4049/jimmunol.1302574
http://www.jimmunol.org/content/193/10/5140

The Journal of Immunology is published twice each month by
The American Association of Immunologists, Inc.,
9650 Rockville Pike, Bethesda, MD 20814-3994.

Print ISSN: 0022-1767 Online ISSN: 1550-6606.

Alarmin Function of Cathelicidin Antimicrobial Peptide LL37 through IL-36γ Induction in Human Epidermal Keratinocytes

Na Li,* Kenshi Yamasaki,* Rumiko Saito,*,† Sawako Fukushi-Takahashi,* Ryoko Shimada-Omori,* Masayuki Asano,* and Setsuya Aiba*

Several dermatoses, including psoriasis, atopic dermatitis, and rosacea, alter the expression of the innate immune effector human cathelicidin antimicrobial peptide (CAMP). To elucidate the roles of aberrant CAMP in dermatoses, we performed cDNA array analysis in CAMP-stimulated human epidermal keratinocytes, the primary cells responding to innate immune stimuli and a major source of CAMP LL37 in skin. Among LL37-inducible genes, IL-1 cluster genes, particularly *IL36G*, are of interest because we observed coordinate increases in CAMP and IL-36γ in the lesional skin of psoriasis, whereas virtually no CAMP or IL-36γ was observed in nonlesional skin and normal skin. The production and release of IL-36γ were up to 20–30 ng/ml in differentiated keratinocytes cultured in high-calcium media. G-protein inhibitor pertussis toxin and p38 inhibitor suppressed IL-36γ induction by LL37. As an alarmin, LL37 induces chemokines, including CXCL1, CXCL8/IL8, CXCL10/IP-10, and CCL20/MIP3a, and IL-36 (10–100 ng/ml) augments the production of these chemokines by LL37. Pretreatment with small interfering RNA against *IL36γ* and IL-36R *IL36R/IL1RL2* and *IL1RAP* suppressed LL37-dependent *IL8*, *CXCL1*, *CXCL10/IP10*, and *CCL20* production in keratinocytes, suggesting that the alarmin function of LL37 was partially dependent on IL-36γ and its receptors. Counting on CAMP induction in innate stimuli, such as in infection and wounding, IL-36γ induction by cathelicidin would explain the mechanism of initiation of skin inflammation and occasional exacerbations of psoriasis and skin diseases by general infection. ***The Journal of Immunology*****, 2014, 193: 5140–5148.**

Cathelicidin is a gene family that is preserved in vertebrates from fishes to mammals. Some mammals have multiple cathelicidin genes; in humans, *CAMP* is the only cathelicidin gene, and it encodes the 18-kDa proprotein hCAP18. LL37 is one form of the mature cathelicidin peptides that are derived from hCAP18 by enzymatic cleavage with kallikreins in human epidermis (1). LL37 forms an α helical structure and has broad antimicrobial properties against bacteria, virus, and fungus (2–5). LL37 kills microbes and exerts "alarmin" activity, which works as a multifunctional innate immune effector that recruits and activates inflammatory cells, including dendritic cells (DC) and monocytes (6). LL37 drives biological responses through epidermal growth factor receptor (EGFR), formyl peptide receptor-like 1 (FPRL1), TLR4, and TLR9 (7–11), resulting in the induction of proinflammatory cytokines and chemokines, such as IL-8 and IL-6, in monocytes, mast cells, and epithelial cells (5, 12–15). Thus, cathelicidin peptides modulate inflammatory cascades, and the effects of cathelicidin stimulation depend on the host cells and tissues that induce, and are affected by, cathelicidin.

Danger signals, such as infection and injury, exacerbate dermatoses, including psoriasis, and the induction of new lesions by injury is known as the Koebner phenomenon. Danger signals provoke the epidermis to produce cathelicidin through TLR2 activation in keratinocytes (16, 17). Aberrant LL37 expression is observed in psoriasis, rosacea, and other skin inflammatory disorders (18–21). In psoriasis, LL37 enables plasmacytoid DC to recognize self-DNA through TLR9 (8) and enables keratinocytes to induce TLR9 and to react against TLR9 ligands (7). Altered cathelicidin peptides are observed in rosacea, and they induce dermatoses resembling rosacea in mouse skin (19). Thus, cathelicidin has roles in the initiation of inflammatory cascades in some diseases, although the functions and roles of cathelicidin peptides differ depending on the type of dermatosis. Hence, it is still generally unknown how the aberrant cathelicidin causes skin diseases, and how cathelicidin acts as an alarmin in epidermal keratinocytes where innate immune responses are initiated has not systematically analyzed.

To understand how aberrant epidermal cathelicidin affects the behavior of keratinocytes and consequent inflammatory reactions by innate immune systems, we performed cDNA array analysis and revealed that LL37 induces molecules related to innate immunity,

*Department of Dermatology, Graduate School of Medicine, Tohoku University, Sendai, Miyagi 980-8574, Japan; and †Department of Integrative Genomics, Tohoku Medical Megabank Organization, Tohoku University, Sendai, Miyagi 980-8574, Japan

Received for publication October 4, 2013. Accepted for publication September 11, 2014.

This work was supported by the Japanese Ministry of Education, Culture, Sports, Science and Technology, the HIROMI Medical Research Foundation, the Gonryo Medical Foundation, the Dermatology International Academic Exchange Foundation, and the Global Center of Excellence Program of the Japanese Ministry of Education, Culture, Sports, Science and Technology.

The sequences presented in this article have been submitted to the Gene Expression Omnibus database (http://www.ncbi.nlm.nih.gov/geo/query/acc.cgi?acc=GSE49472) under accession number GSE49472.

Address correspondence and reprint requests to Dr. Kenshi Yamasaki, Department of Dermatology, Tohoku University Graduate School of Medicine, Seiryo-machi 1-1, Sendai, Miyagi 980-8574, Japan. E-mail address: kyamasaki@med.tohoku.ac.jp

The online version of this article contains supplemental material.

Abbreviations used in this article: BAF, bafilomycin A1; CAMP, cathelicidin antimicrobial peptide; ChQ, chloroquine diphosphate salt; DC, dendritic cell; EGF, epidermal growth factor; EGFR, epidermal growth factor receptor; FPRL1, formyl peptide receptor-like 1; GPCR, G protein–coupled receptor; HB-EGF, heparin-binding EGF-like growth factor; hCAMP, human cathelicidin antimicrobial peptide; PBST, 0.05% Tween 20 in PBS; PTx, pertussis toxin; RT, room temperature; siRNA, small interfering RNA.

www.jimmunol.org/cgi/doi/10.4049/jimmunol.1302574

such as the IL-1 family and antimicrobial peptides, as well as chemokines in human keratinocytes. Among them, IL-36γ is of particular interest because IL-36γ and LL37 are abundant in psoriasis epidermis, and they synergistically increase chemokine production in human keratinocytes. Furthermore, silencing of IL-36γ and its receptors attenuated LL-37–dependent chemokine induction in keratinocytes, suggesting that LL37 initiates and exacerbates inflammation coordinately with IL-36γ and that IL-36γ enhances the alarmin functions of epidermis in dermatoses.

Materials and Methods

Cells, media, and reagents

Human neonatal epidermal keratinocytes were grown in serum-free medium supplemented with HuMedia-KG2 Growth Supplements (KURABO INDUSTRIES, Tokyo, Japan). All cells were passed at 80% confluence under low-calcium conditions (0.05 mM), and keratinocytes in the third or fourth passage were used for the experiments. To induce keratinocyte differentiation, confluent keratinocytes were cultured in 1 mM calcium media for 72 h; subsequently, the calcium concentration was increased to 1.6 mM for an additional 48 h. Human cathelicidin antimicrobial peptide (hCAMP) LL37 (amino acid sequence of LLGDFFRKSKEKIGKEFKRIVQRIKDFLRNLVPRTES) was synthesized by Scrum (Tokyo, Japan). Recombinant human IL-36 (IL-36α, β, and γ), monoclonal rat anti-human IL-36γ/IL-1F9 Ab (MAB2320), and human IL-36γ/IL-1F9 biotinylated Ab (BAF2320) were purchased from R&D Systems (Minneapolis, MN). Polyclonal goat anti-human IL-36γ/IL-1F9 Ab was purchased from Santa Cruz Biotechnology (Dallas, TX). P38 MAPK inhibitor SB203580, MEK inhibitor PD98059, rhodamine-conjugated donkey anti-goat IgG were purchased from Chemicon International (Temecula, CA). FITC-conjugated donkey anti-rabbit IgG, and G_i protein inhibitor pertussis toxin (PTx) were purchased from Merck Millipore (Billerica, MA). JNK1/2 inhibitor SP600125, heparin-binding EGF-like growth factor (HB-EGF) inhibitor CRM197 (nontoxic mutant of diphtheria toxin solution), and EGFR tyrosine kinase inhibitor AG1478 were purchased from Wako Pure Chemical Industries (Osaka, Japan). The NF-κB inhibitor curcumin and the endosomal acidification inhibitors chloroquine diphosphate salt (ChQ) and bafilomycin A1 (BAF) were purchased from Sigma-Aldrich (St. Louis, MO). TLR2 and TLR4 inhibitor OxPAPC, TLR9 antagonist ODN TTAGGG (ODN A151), and ODN TTAGGG control were purchased from InvivoGen (San Diego, CA).

DNA microarray

Keratinocytes were maintained in an undifferentiated condition in low-calcium media (0.05 mM) or in a differentiated condition in high-calcium media (1.6 mM) and stimulated with LL37 at 0, 2.56, or 7.68 μM for 12 or 24 h. Total RNA was isolated using an RNeasy Mini Kit and the RNase-Free DNase set (both from QIAGEN, Valencia, CA). Total RNA concentration was measured using a NanoDrop spectrophotometer (Thermo Fisher Scientific, Waltham, MA). The RNA quality was determined using the RNA 6000 Nano Kit and an Agilent 2100 Bioanalyzer (both from Agilent Technologies, Palo Alto, CA), and the RNA Integrity Number was confirmed to be ≥9. Total RNA was amplified, labeled, and analyzed as previously described (22). Normalization of the expression data was performed using GeneSpring GX 12.6 (Agilent Technologies) to query the expression of 41,000 genes with 44,000 distinct probes. After data transformation to GeneSpring, per-chip normalization to the 75th percentile and baseline to the median of all samples was performed. After this normalization, extremely low-intensity probes were excluded, leaving 32,940 probes for analysis. The cDNA microarray data were deposited in the Gene Expression Omnibus

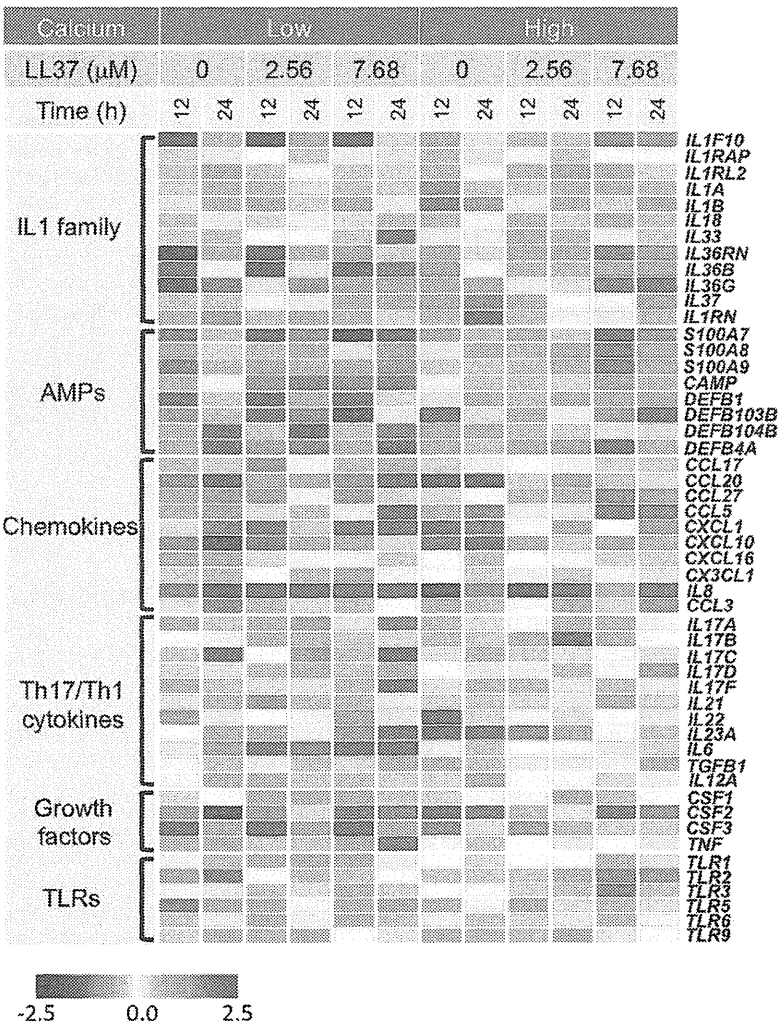

FIGURE 1. LL37 altered innate immune gene expression in undifferentiated and differentiated keratinocytes. Undifferentiated keratinocytes (low calcium; 0.05 mM) and differentiated keratinocytes (high calcium; 1.6 mM) were stimulated with hCAMP LL37 at 0, 2.56, or 7.68 μM for 12 or 24 h. Individual boxes represent the relative gene expression intensity (log_2-transformed signal ratios of the replicate spots) of the given genes (rows) in each culture condition. The color bar shows the log_2 ratio.

database under accession number GSE49472 (http://www.ncbi.nlm.nih.gov/geo/query/acc.cgi?acc=GSE49472).

RNA isolation and quantitative RT-PCR

Total RNA was extracted using ISOGEN (NIPPON GENE, Toyama, Japan). cDNA synthesis and quantitative PCR were performed as previously described (23). The primers and TaqMan probe sets used are listed in Supplemental Table I.

Western blotting

Cells were lysed in RIPA buffer (50 mM HEPES, 150 mM NaCl, 0.05% SDS, 0.25% deoxycholate, 0.5% Nonidet P-40 [pH 7.4]) with cOmplete protease inhibitors (F. Hoffmann-La Roche, Basel, Switzerland). The protein concentration was determined using the Pierce BCA kit (Thermo Fisher Scientific). A total of 20 μg total protein or recombinant human IL-36γ/IL-1F9 (aa 18–169) was loaded/well for electroporation and Western blotting. Membranes were incubated at 4°C overnight with monoclonal rat anti-human IL-36γ/IL-1F9 Ab (1 μg/ml), rinsed with TBS-T (25 mM Tris [pH 7.5] and 0.1% Tween 20), and incubated with HRP-labeled polyclonal goat anti-rat IgG Ab. Chemiluminescence data from Western blots were collected using an Image Quant LAS 4000 mini (GE Healthcare UK, Little Chalfont, U.K.).

ELISA and Bio-Plex assay to measure proteins in culture media

IL-36γ protein in the supernatants of the keratinocytes was measured by sandwich ELISA. Microlon 96-well high-binding plates (Greiner Bio-One, Frickenhausen, Germany) were coated with 100 μl/well monoclonal rat anti-human IL-36γ/IL-1F9 Ab (1 μg/ml) overnight at room temperature (RT). After washing thrice with 0.05% Tween 20 in PBS (PBST), 300 μl blocking solution containing 5% BSA in PBST was added for 1 h at RT. After washing with PBST, 100 μl samples or rIL-36γ/IL-1F9 was added to each well in duplicate and incubated for 2 h at RT. After washing with PBST, human IL-36γ/IL-1F9 biotinylated Ab (0.5 μg/ml in PBST) was added for 2 h at RT. Streptavidin-HRP and substrate solution was used for colorimetric assay following the manufacturer's instructions (R&D Systems).

To detect multiple cytokines and chemokines in the supernatants of keratinocytes stimulated with IL-36 in the presence or absence of LL37, Bio-Plex Pro Human Cytokine Assay 1 × 96-well 27-Plex Group I and Bio-Plex suspension array system (both from Bio-Rad, Hercules, CA) were used, following the manufacturer's instructions. IL-8, CXCL1, and CCL20 protein in cultured media were measured using a DuoSet ELISA Development human kit (R&D Systems).

Immunohistochemistry and immunofluorescence staining

Paraffin sections (3 μm thickness) were treated with a microwave, blocked with rabbit serum (Sigma-Aldrich), and incubated with polyclonal goat anti-human IL-36γ/IL-1F9 Ab (20 μg/ml) at 4°C overnight. Subsequently, sections were visualized with a Histofine SAB-PO (G) kit (Nichirei Biosciences, Tokyo, Japan) and 3,3′-diaminobenzidine substrate (Wako Pure Chemical Industries) and counterstained with Mayer's hematoxylin. Images were obtained using an Axio Imager M1 microscope (Carl-Zeiss, Oberkochen, Germany).

For immunofluorescence, paraffin sections were incubated with polyclonal goat anti-human IL-36γ/IL-1F9 Ab and polyclonal rabbit anti-human LL37 Ab (Phoenix Pharmaceuticals, Burlingame, CA) at 4°C overnight. Rhodamine-conjugated donkey anti-goat IgG and FITC-conjugated donkey anti-rabbit IgG were used as secondary Abs. Images were obtained using a Zeiss LSM700 laser scanning confocal microscope (Carl-Zeiss).

Small interfering RNA

The small interfering RNA (siRNA) for IL36B, IL36G, IL36RN, IL1RL2 (IL36R), and IL1RAP (FlexiTube GeneSolution; GS27177 for IL36B, GS56300 for IL36G, GS26525 for IL36RN, GS8808 for IL1RL2, and GS3556 for IL1RAP), control siRNA (AllStars Negative Control siRNA), and HiPerFect Transfection Reagent (both from QIAGEN) were used for the siRNA experiments. Keratinocytes were processed with siRNA (10 nM) following the protocol in the HiPerFect Transfection Reagent handbook (QIAGEN). After 24 h for gene silencing, LL37 (0, 2.56, or 7.68 μM) was added to each well. After 24 h of stimulation, the supernatants were collected for protein analysis, and the total RNA was isolated as described above.

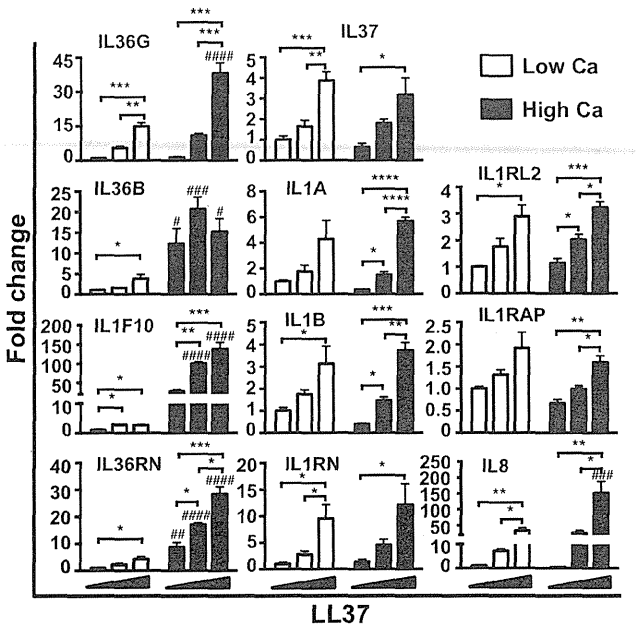

FIGURE 2. LL37 increases gene expression of IL-1 family and IL-36R. Keratinocytes were cultured in low-calcium or high-calcium media and stimulated with LL37 (0, 2.56, or 7.58 μM from left to right) for 24 h. Gene expression is indicated as the fold change compared with keratinocytes cultured in low-calcium media without LL37 (mean ± SEM, $n = 3$). $^{*}p < 0.05$, $^{**}p < 0.01$, $^{***}p < 0.001$, $^{****}p < 0.0001$. $^{\#}p < 0.05$, $^{\#\#}p < 0.01$, $^{\#\#\#}p < 0.001$, $^{\#\#\#\#}p < 0.0001$ versus low-calcium condition.

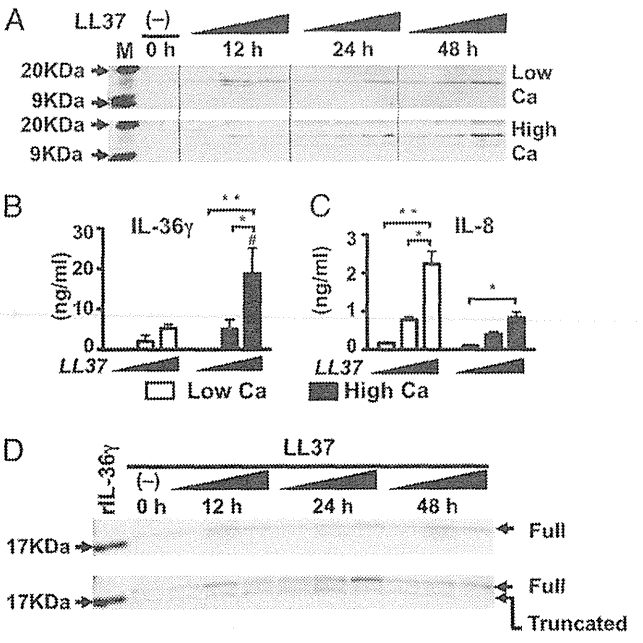

FIGURE 3. LL37 increases IL-36γ protein expression and release from keratinocytes. (**A**) Keratinocytes were treated with LL37 (0, 2.56, 7.68 μM, left to right lanes) for 12, 24, or 48 h in low-calcium (*upper panel*) or high-calcium (*lower panel*) conditions. Cellular IL-36γ was detected by Western blotting. (**B** and **C**) The keratinocyte culture media were collected at 24 h after stimulation with LL37 at 0, 2.56, and 7.68 μM (left to right bars). IL-36γ (B) and IL-8 (C) in culture supernatant were measured by ELISA (mean ± SEM, $n = 3$). (**D**) Keratinocytes were treated with LL37 (0, 2.56, or 7.68 μM, left to right bars) for 12, 24, or 48 h in low-calcium (*upper panel*) or high-calcium (*lower panel*) conditions. Cellular IL-36γ was detected by Western blotting. Recombinant human IL-36γ/IL-1F9 (a truncated form, aa 18–169) was used as a positive control. $^{*}p < 0.05$, $^{**}p < 0.01$. $^{\#}p < 0.05$ versus low-calcium condition.

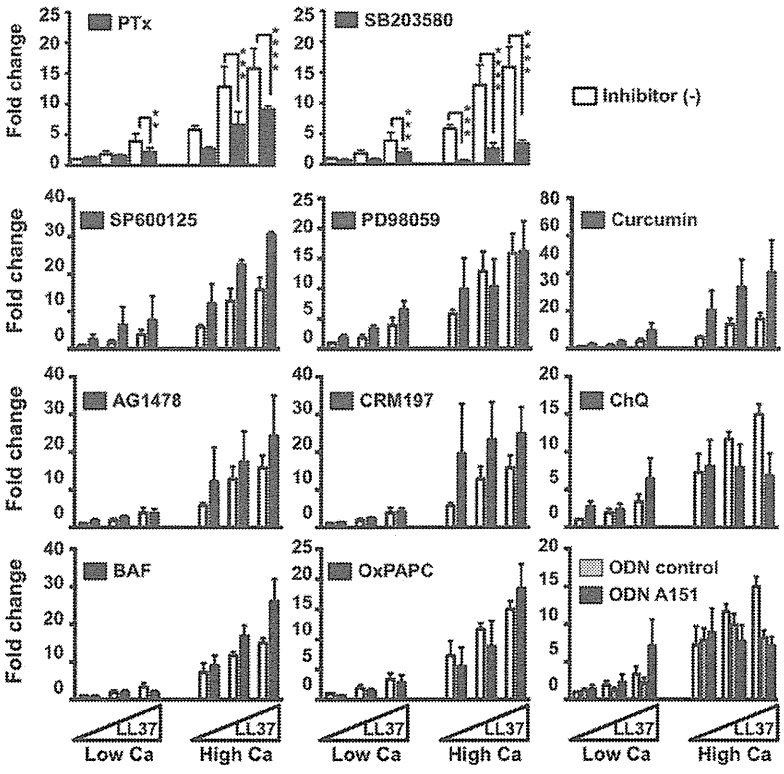

FIGURE 4. LL37 induces *IL36G* through G_i protein-coupled signals and p38 MAPK signals. Keratinocytes cultured in low-calcium media (the left side) or high-calcium media (*right side*) were treated (black bars) or not (vehicle controls, white bars) with the indicated inhibitors for 1 h at 37°C and then stimulated with LL37 at 0, 2.56, or 7.68 μM for 24 h. The inhibitors used were G_i protein inhibitor PTx, p38 kinase–specific inhibitor SB203580, JNK1/2 inhibitor SP600125, MEK inhibitor PD98059, NF-κB inhibitor curcumin, EGFR tyrosine kinase inhibitor AG1478, HB-EGF inhibitor CRM197, endosomal acidification inhibitors ChQ and BAF, TLR2 and TLR4 inhibitor OxPAPC, TLR9 antagonist ODN A151, and ODN control. Total RNA was collected to measure *IL36G* by quantitative RT-PCR. Gene expression is represented as the fold change relative to keratinocytes that were not treated with inhibitors and not stimulated with LL37. Data are mean ± SEM of three independent experiments. $^{**}p < 0.01$, $^{***}p < 0.001$, $^{****}p < 0.0001$.

Inhibition of EGFR, G_i protein, TLRs, and intracellular signaling pathway

To determine the signaling pathway by which LL37 induces *IL36G*, the keratinocytes were pretreated with inhibitors for 1 h and stimulated with LL37 at 0, 2.56, or 7.68 μM for 24 h in both low- and high-calcium conditions. The inhibitors used for the assay were HB-EGF inhibitor CRM197 (10 μg/ml), EGFR tyrosine kinase inhibitor AG1478 (50 nM), Gi protein inhibitor PTx (200 ng/ml), endosomal acidification inhibitors ChQ (5 μM) and BAF (100 nM), p38 MAPK inhibitor SB203580 (10 μM), MEK inhibitor PD98059 (20 μM), JNK1/2 inhibitor SP600125 (10 μM), NF-κB inhibitor curcumin (10 μM), TLR2 and TLR4 inhibitor OxPAPC (30 μg/ml), and TLR9 antagonist ODN TTAGGG (ODN A151, 1 μM) and ODN TTAGGG control (1 μM). Total RNA was collected to measure *IL36G* using quantitative RT-PCR.

To determine the signaling pathway by which IL-36γ induces chemokine induction, keratinocytes were pretreated with p38 MAPK inhibitor SB203580 (10 μM), MEK inhibitor PD98059 (20 μM), JNK1/2 inhibitor SP600125 (10 μM), or NF-κB inhibitor curcumin (10 μM) for 1 h and stimulated with 100 ng/ml IL-36 (α, β, γ) in the presence or absence of LL37 (2.56 μM) for 24 h under low-calcium conditions. Total RNA was collected to measure *IL8*, *CXCL10*, *CXCL1*, and *CCL20* by quantitative RT-PCR.

Statistical analysis

Data were analyzed by one-way ANOVA with the Tukey multiple-comparisons test or two-way ANOVA with the Sidak multiple-comparisons test using GraphPad Prism 6 (GraphPad, La Jolla, CA), unless otherwise stated. The p values < 0.05 were considered significant. All experiments were performed in triplicate and repeated at least three times to confirm the reproducibility.

Results

hCAMP LL37 augments the expression of IL-36γ and IL-1 cluster genes in human keratinocytes

Because the cathelicidin peptide LL37 modifies the host immune responses, cell growth, migration, and differentiation (24), we conducted cDNA microarray analysis to understand the consequences of aberrant cathelicidin antimicrobial peptide (CAMP) expression in epidermal keratinocytes of dermatoses. We stimulated human epidermal keratinocytes with LL37 (2.56 or 7.68 μM) for 12 or 24 h and identified genes with altered expression in both undifferentiated keratinocytes (low calcium) and differenti-

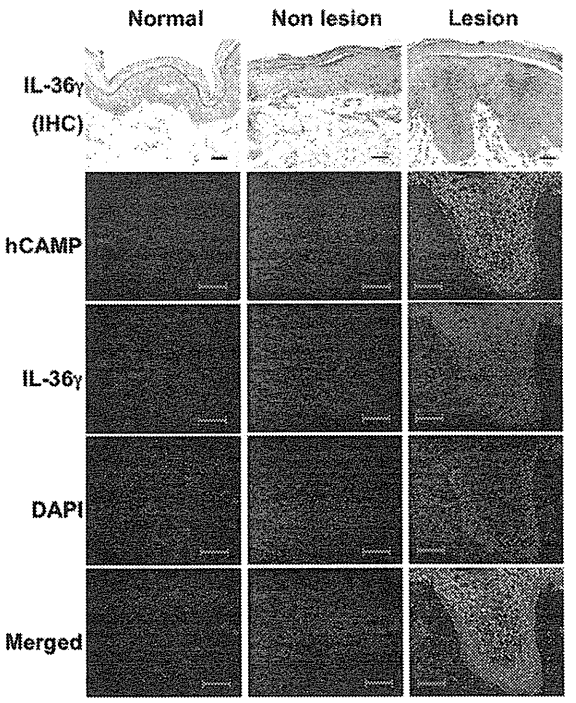

FIGURE 5. Coordinate increases in IL-36γ and CAMP (LL37) in lesional epidermis of psoriasis. Localization of hCAMP and IL-36γ was visualized by immunohistochemical staining (*top three panels*; scale bars, 500 μm) or by immunofluorescence (*all lower panels*; scale bars, 50 μm) in normal human skin, nonlesional skin of a psoriasis patient, or lesional skin of a psoriasis patient. Green indicates cathelicidin (LL37), red indicates IL-36γ, and nuclei were visualized with DAPI (blue).

ated keratinocytes (high calcium). These LL37 concentrations were the ones observed in skin diseases (19, 20). *IL8* induction confirmed a proper stimulation by LL37 (13) (Supplemental Table II). From the microarray data, we identified several gene groups that affect inflammatory reactions in skin diseases (5, 25–28). LL37 increased genes of the IL-1 family, antimicrobial peptides, and chemokines in keratinocytes (Fig. 1). Increases in the IL-1 family and antimicrobial peptides were more obvious in differentiated keratinocytes cultured in high-calcium media. LL37 increased Th17/Th1-related genes *IL6* and *IL23A* and increased *CSF2* (GM-CSF) in undifferentiated keratinocytes. We did not observe significant expression of *IL10* or Th2 cytokines *IL4* and *IL13* by keratinocytes (data not shown). Most of the TLRs were increased in differentiated keratinocytes, and LL37 increased *TLR2*. Thus, LL37 induced proinflammatory cytokines related to the IL-1 family, Th1/Th17 cascades, and innate immune molecules antimicrobial peptides and TLRs.

The IL-1 family contains 11 members: IL-1α, IL-1β, IL-1R antagonist (IL-1RN), IL-18, IL-33, IL36RN/IL-1F5, IL-36α/IL-1F6, IL-36β/IL-1F8, IL-36γ/IL-1F9, IL-37/IL-1F7, and IL-1F10/IL-38 (29). LL37 increased *IL36G*, *IL36RN*, *IL1F10*, *IL1A*, *IL1B*, and *IL1RN* in both undifferentiated and differentiated keratinocytes, and it increased *IL36B* and *IL37* in differentiated keratinocytes. *IL36γ* was significantly increased (>4-fold) by LL37 in both undifferentiated and differentiated keratinocytes (Supplemental Table II). Quantitative RT-PCR confirmed the induction of IL-1 cluster genes by LL37 (Fig. 2). *IL36G*, *IL36B*, *IL1F10*, and *IL36RN* were increased by LL37, and the high-calcium condition augmented their expression. *IL37*, *IL1A IL1B*, and *IL1RN* were increased by LL37, and the calcium conditions had virtually no effect on their expression. We also observed that LL37 increased the IL-36R *IL1RL2/IL36R* and *IL1RAP*. Consistent with the very low level of *IL36A* in the microarray analysis, *IL36A* was not detectable by quantitative RT-PCR (data not shown).

Because LL37 stimulation induced IL-36γ mRNA most significantly in the IL-1 cluster genes, we further examined the dynamics of IL-36γ. We observed that LL37 increased IL-36γ protein in a time- and a dose-dependent manner (Fig. 3A). IL-36γ release in cultured media was confirmed by ELISA (Fig. 3B). In parallel with the calcium effects on *IL36G* mRNA, IL-36γ protein was increased in the high-calcium condition. Truncated forms of IL-36γ have greater immunological activity than do their full-length counterparts (30). Keratinocytes stimulated by LL37, especially differentiated keratinocytes, produced both the full-length and the truncated active forms of IL-36γ (Fig. 3D). These data showed that cathelicidin augmented IL-36γ expression in keratinocytes and that calcium modulated the expression. Again, IL-8 served as positive controls for LL37 stimuli (Fig. 3C).

LL37 induces IL-36γ through G_i protein–coupled signaling and p38 MAPK

LL37 acts on several receptors and signaling pathways, including EGFR, FPRL1, TLR4, and TLR9, to induce proinflammatory cytokines and chemokines (5, 7–15). We examined which signaling pathways are involved in *IL36G* induction by LL37. PTx, a reagent known to selectively block G_i protein–coupled signaling, significantly decreased *IL36G* induction by LL37 in both undifferentiated and differentiated keratinocytes (Fig. 4). EGFR inhibition by HB-EGF inhibitor CRM197 and EGFR tyrosine kinase inhibitor AG1478, as well as blockade of TLRs by TLR2 and TLR4 inhibitor OxPAPC and TLR9 antagonist ODN TTAGGG, did not affect *IL36G* induction by LL37. Among the intracellular signaling pathways, p38 MAPK–specific inhibitor SB203580 blocked *IL36G* induction by LL37. JNK inhibitor SP600125, MEK inhibitor PD98059, NF-κB inhibitor curcumin, and endosomal acidification inhibitors ChQ and BAF did not affect *IL36G* induction by LL37. These observations suggest that LL37 induces *IL36G* through a G_i protein–coupled receptor (GPCR) and p38 MAPK–signaling pathway in human epidermal keratinocytes.

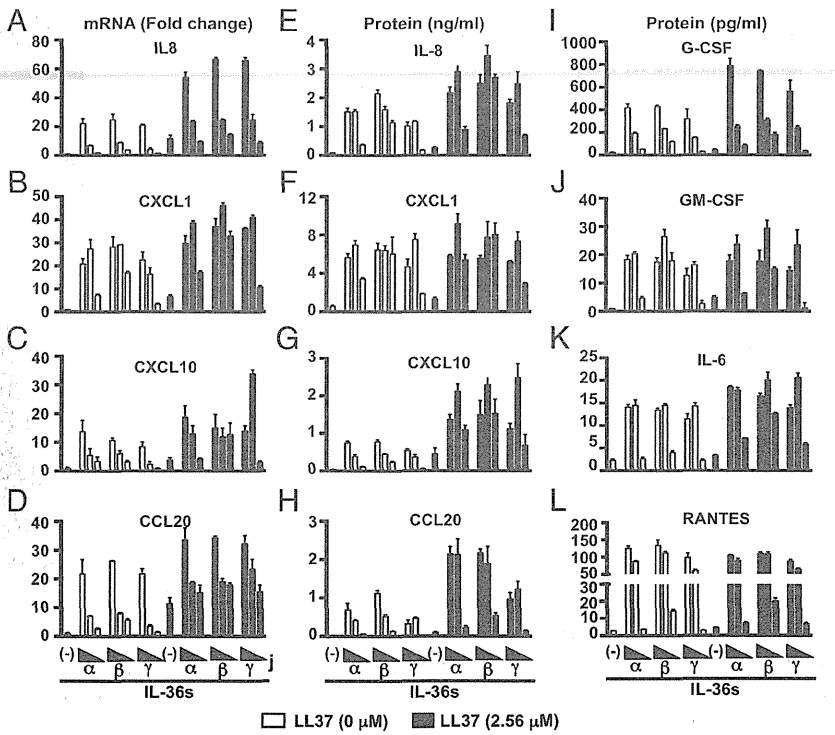

FIGURE 6. Induction of chemokines and cytokines by LL37 and IL-36. (**A–D**) Keratinocytes were cultured in a low-calcium condition, stimulated with IL-36 (α, β, γ) at 1 μg/ml, 100 ng/ml, or 10 ng/ml (left to right bars) in the absence (white bars) or presence (black bars) of LL37 (2.56 μM) for 24 h. Gene expression is represented as the fold change relative to keratinocytes that were not cultured with IL-36 and LL37 (mean ± SEM, $n = 3$). (**E–L**) Keratinocytes were stimulated as described above, and proteins in the culture supernatants were analyzed by Bio-Plex multiplex analyses or sandwich ELISA. Data are mean ± SEM of three independent experiments.

IL-36γ is abundant and coexists with hCAMP in psoriasis epidermis

Because hCAMP is abundantly expressed in psoriatic epidermis (7, 18, 20), we examined the expression of hCAMP and IL-36γ in psoriatic skin. As reported previously (31, 32), we observed high IL-36γ expression in the lesional epidermis of psoriasis (Fig. 5). We also confirmed that IL-36γ and LL37 coexisted in the lesional skin of psoriasis. It is noteworthy that IL-36γ was observed more in suprabasal cells than in basal cells, which is consistent with the in vitro data showing greater IL-36γ induction by LL37 in differentiated keratinocytes in high-calcium condition (Figs. 2, 3).

LL37 and IL-36 coordinately increase chemokines and cytokines in keratinocytes

To elucidate how the coexistence of abundant IL-36γ and LL37 affects the epidermis, we stimulated keratinocytes with LL37 and IL-36 and examined the induction of chemokines and cytokines using cDNA array analysis (Supplemental Table III). Exogenous IL-36α, β, and γ increased IL-8, CXCL1, CXCL10, and CCL20 mRNA in a dose-dependent manner at concentrations of 10 ng/ml to 1 μg/ml (Fig. 6A–D). Chemokine release by IL-36 also was observed, and 100 ng/ml of IL-36 efficiently increased the release of most chemokines (Fig. 6E–H). Because up to 30 ng/ml of IL-36γ was detected from keratinocytes in vitro (Fig. 3B), it is suggested that a physiological concentration of IL-36 released from keratinocytes would result in skin inflammation through chemokine induction. The presence of LL37 further augmented the production of CXCL10, CCL20, and G-CSF (CSF3) but showed little effect on CXCL1, GM-CSF (CSF2), IL-6, and RANTES (CCL5).

To explore the intracellular signaling pathways that induce chemokines by IL-36 and LL37, we treated keratinocytes with inhibitors for MAPK or NF-κB. p38 MAPK inhibitor SB203580 suppressed IL-36–derived *IL8*, *CXCL10*, and *CCL20* expression, regardless of the presence of LL37 (Supplemental Fig. 1). The NF-κB inhibitor curcumin significantly suppressed *CXCL1* and *CXCL10* expression by IL-36, regardless of the presence of LL37. The JNK1/2 inhibitor SP600125 reduced *IL8* and *CXCL1* expression induced by IL-36, but it augmented *CXCL10* and *CCL20* expression (Supplemental Fig. 1). The MEK1/2 inhibitor PD98059 showed no effect on *IL8* and *CXCL1* but augmented *CXCL10* and *CCL20* expression (Supplemental Fig. 1). Thus, LL37 and IL-36 coordinately augment the production of these chemokines, primarily through p38 and JNK MAPK and NF-κB pathways, and MEK1/2 signaling negatively regulates the expression of these chemokines in keratinocytes.

LL37 induces chemokines through IL-36γ and IL-36R in keratinocytes

Associating the IL-36γ induction by LL37 with the IL-36γ–inducible chemokines from keratinocytes, we sought to determine

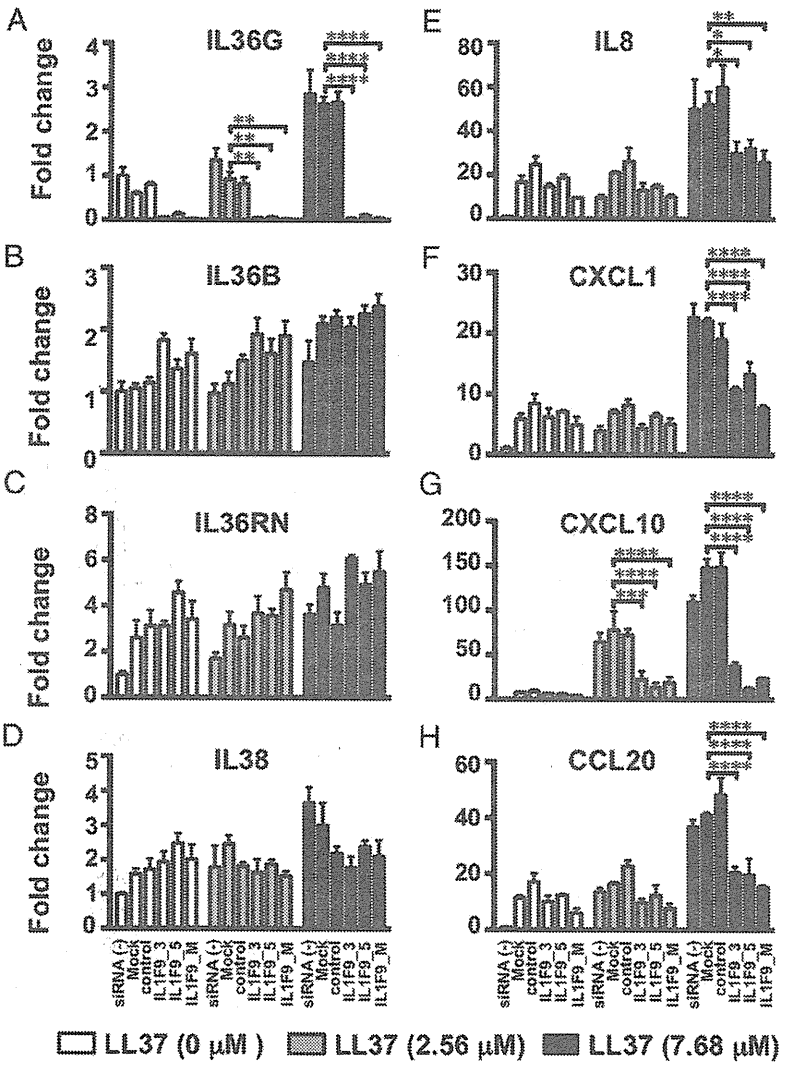

FIGURE 7. LL37 induces chemokines through IL-36γ induction in keratinocytes. (**A–H**) Keratinocytes were not treated with siRNA [siRNA (−)] or were treated with transfection reagent only (mock), siRNA against control RNA (control), or siRNA against *IL36G* (IL1F9_3, IL1F9_5, or IL1F9_Mix) for 24 h and then stimulated with LL37 (0 μM, white bars; 2.56 μM, gray bars; 7.68 μM, black bars) for 24 h in low-calcium condition. Gene expression is represented as the fold change relative to keratinocytes that were not pretreated with siRNA [siRNA (−)] and not stimulated with LL37. Data are mean ± SEM of three independent experiments. $*p < 0.05$, $**p < 0.01$, $***p < 0.001$, $****p < 0.0001$ versus mock-treated sample.

whether LL37 induces chemokines that are dependent on IL-36γ induction. We knocked down *IL36G/IL1F9* by siRNA (IL1F9_3, IL1F9_5, and IL1F9_Mix) for 24 h and then stimulated it with LL37 for another 24 h. *IL36G* suppression was confirmed in LL37-treated keratinocytes (Fig. 7A). The stable *IL36B* expression showed the specificity of *IL36G* siRNA (Fig. 7B). *IL36G* siRNA (IL1F9_3, IL1F9_5, and IL1F9_Mix) significantly suppressed *IL8*, *CXCL1*, CXCL10, and *CCL20* induction by LL37 (Fig. 7E–H). Silencing of IL-36R *IL36R/IL1RL2* and *IL1RAP* also significantly decreased the induction of chemokines by LL37 (Fig. 8). Expression of *IL36RN* and *IL38/IL1F10*, which are known antagonists of IL-36 ligands, was not altered when *IL36G* was silenced (Fig. 7C, 7D). *IL36RN* knock down did not significantly alter chemokine induction by LL37 (Fig. 8). These results suggested that LL37 induces chemokines in keratinocytes, at least in part, via an IL-36γ and IL-36R–mediated mechanism, and IL-36 antagonist IL-36RN has little effect on chemokine induction by LL37.

Discussion

In this study, we systematically examined the LL37-inducible genes in human keratinocytes by cDNA array analysis and demonstrated that a representative hCAMP LL37 induces IL-1 cluster genes, antimicrobial peptides, and chemokines. Among IL-1 cluster genes, we showed that LL37 induces IL-36γ in both undifferentiated and differentiated keratinocytes and that IL-36γ and hCAMP are both abundant and coexisted in psoriatic epidermis. IL-36γ and LL37 coordinately induced chemokine production from human epidermal keratinocytes. Furthermore, the induction of proinflammatory cytokines and chemokines by LL37 is carried out, at least in part, through IL-36γ induction and the IL-36R pathway. Thus, this study revealed that alarmin functions of LL37 in human epidermis are enhanced by IL-36γ induction and its receptors in keratinocytes, as well as through the induction of other molecules related to the innate immune reaction.

The Koebner phenomenon is well known in psoriasis: danger signals, such as infection and injury, provoke new skin lesions in psoriasis patients. Because cathelicidin can be induced in human epidermis by environmental changes, including infections and injuries, the coexistence of LL37 and IL-36γ in psoriatic epidermis would initiate skin exacerbations by stimuli from the microenvironment. IL-36γ and IL-36β are increased in human psoriatic epidermis (32), whereas IL-36α–transgenic mice show an inflammatory skin condition that is similar to human psoriasis (31). In patients with a familial history of generalized pustular psoriasis, homozygous loss-of-function mutations were identified in IL-36R antagonist (IL-36RN), which results in constitutive IL-36 activation (33, 34). Thus, the possible involvement of IL-36 signaling has gained attention in the pathogenesis of psoriasis. Our data showed that LL37 induces IL-36γ and that IL-36 efficiently induces chemokines and cytokines in the presence of LL37 in human keratinocytes. IL-36–inducible factors from human keratinocytes include chemokines IL-8, CXCL1, CXCL10, RANTES,

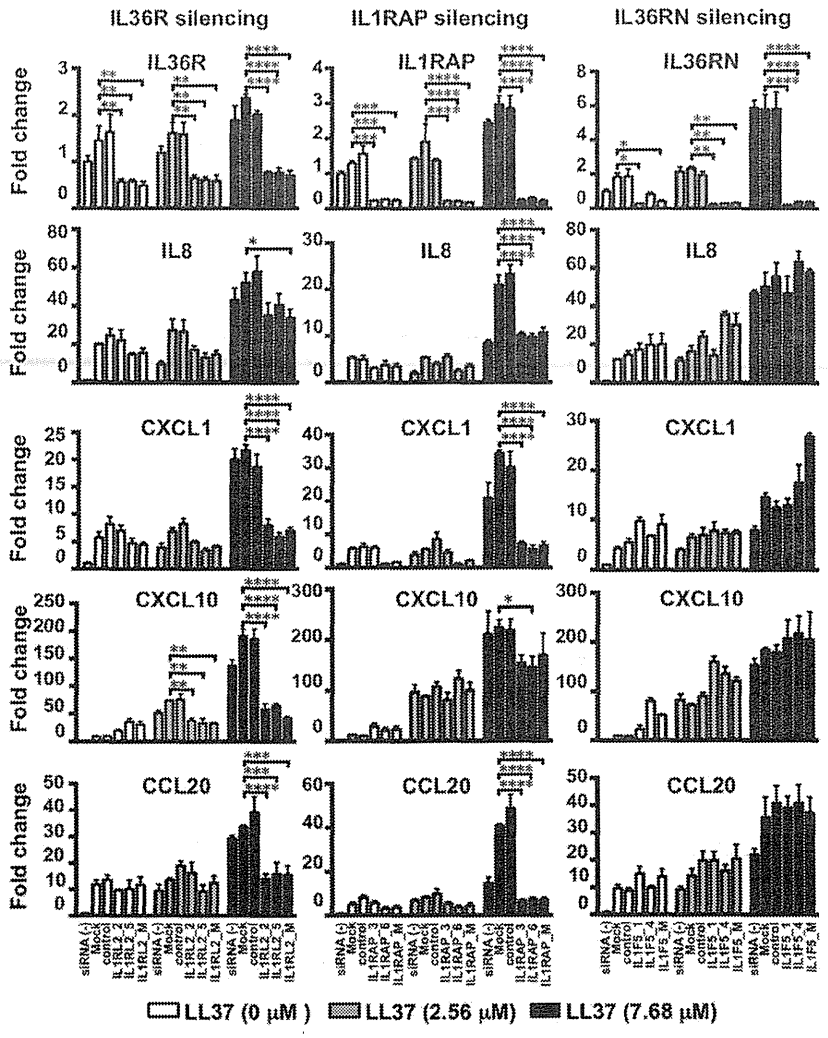

FIGURE 8. LL37 induces chemokines dependent on IL-36R but not IL-36RN in keratinocytes. Keratinocytes were not treated with siRNA [siRNA (−)] or were treated with transfection reagent only (mock), siRNA against control RNA (control), or siRNA (IL1RL2_2, IL1RL2_5, and IL1RL2_M for IL1RL2/IL36R; IL1RAP_3, IL1RAP_6, and IL1RAP_M for IL1RAP; IL1F5_1, IL1F5_4, IL1F5_M for IL36RN) for 24 h. Subsequently, the keratinocytes were stimulated with LL37 (0 μM, white bars; 2.56 μM, gray bars; 7.68 μM, black bars) for 24 h in low-calcium condition. Gene expression is represented as the fold change relative to keratinocytes that were not treated with siRNA [siRNA (−)] and not stimulated with LL37. Data are mean ± SEM of three independent experiments. $*p < 0.05$, $**p < 0.01$, $***p < 0.001$, $****p < 0.0001$ versus mock-treated sample.

and CCL20, and cytokines IL-6, G-CSF, and GM-CSF, which can recruit and activate DC, macrophages, neutrophils, T cells, and NK cells. Studies in other epithelial tissues, such as human bronchial epithelial cells and mouse lungs, showed that IL-36, particularly IL-36γ, induces the neutrophil-attracting chemokines IL-8 and CXCL1, the T cell–attracting chemokines CXCL10, and the DC-attracting and Th17-attracting chemokine CCL20, as well as cytokines and growth factors, including IL-6, G-CSF, and GM-CSF (35, 36). Data from previous studies combined with our data indicate that IL-36γ would activate epithelial cells to induce chemokines and recruit inflammatory cells for the initial stages of innate immunity in skin inflammation. Thus, in human epidermal keratinocytes, the induction of CAMP by innate immune stimuli can be a trigger to activate the IL-36 axis that initiates skin inflammation and exacerbates chronic dermatoses.

The cathelicidin LL37 acts on several receptors and signaling pathways (5, 7–15). By blocking with PTx, we demonstrated that LL37 induced *IL36G* through G_i protein–coupled signaling. Among GPCR, LL37 is known to activate FPRL1 in endothelial cells (10). However, keratinocytes are suggested to have little FPRL1 and induce transactivation of EGFR by LL37, which is mediated through GPCR other than FPRL1 (13). However, we observed that EGFR inhibition by HB-EGF inhibitor CRM197 and EGFR tyrosine kinase inhibitor AG1478 did not affect *IL36G* induction by LL37. Because EGFR dominantly activates p42/p44 MEK in keratinocytes, inhibition of LL37-mediated *IL36G* induction by p38 inhibitor SB203580, but not by MEK inhibitor PD98059, also suggested little involvement of EGFR in *IL36G* induction by LL37 in keratinocytes. Although specific receptors inducing *IL36G* by LL37 were not identified in this study, multiple GPCR might be involved in the process. The ligand-dependent and -independent activation and oligomerization of GPCR are recognized as a cross-talk of GPCR, which alters intracellular signals making them different from the non-oligomerized GPCR signaling (37–40). Because LL37 is a cationic peptide and can bind directly to the cell membrane without receptors (8, 41), it may activate GPCR in a ligand-independent manner to induce IL-36γ. Occasionally, we observed increases in chemokines when we treated keratinocytes with mock (transfection reagent) and control siRNA along with LL37 (Figs. 7, 8). These phenomena also suggested the ligand-independent activation of GPCR, because the transfection reagent is also a cation that affects cell membrane components. The molecular mechanism of LL37-mediated GPCR activation should be explored further to define the cascade of inflammatory reactions in innate immunity of the skin.

We demonstrated that LL37 induces IL-36R IL-1RL2/IL-36R and IL-1RAP, as well as IL-36γ, IL-36β, and other IL-1 family genes. Therefore, LL37 would amplify the stimulation of IL-36 by inducing both ligands and their receptors in keratinocytes, which was demonstrated, in part, by the experiments with siRNA for *IL36G* and its receptors *IL36R/IL1RL2* and *IL1RAP*. We also showed that p38 and JNK MAPK and NF-κB signaling affected the induction of chemokines in combination with IL-36 and LL37; these results are similar to those from a previous study that demonstrated that IL-36 phosphorylates NF-κB and JNK and p38 MAPK (30). IL-1β and IL-1R–associated kinase-1 are aberrantly expressed in psoriatic lesions, and the synergy between IL-1β and TNF-α leads to sustained inflammatory responses (42). IL-18 induces IFN-γ, and the increased IL-18 participates in the development of the Th1 response in lesional skin of psoriasis (43). IL-36α, IL-36β, and IL-36γ are members of IL-1 family of cytokines and use the same receptor IL-36R/IL-1RL2 coupled with IL-1RAP (30), and IL-36 induces TNF and IL-6 in human keratinocytes (44). Combined with observations of the functions of IL-1 family molecules in psoriasis, cathelicidin-dependent induction of IL-1 family molecules might indicate that the mechanism of altered innate immunity exacerbates and modulates inflammatory responses in psoriasis.

In summary, hCAMP LL37 induces IL-36γ production, as well as IL-36R. LL37 induces IL-8, CXCL1, CXCL10, and CCL20 through IL-36γ induction and IL-36R signaling, which would recruit neutrophils, T cells (including Th17 cells), and DC for the epidermis. Our findings provide evidence that some of the alarmin activities of LL37 occur via IL-36γ induction; thus, IL-36γ facilitates innate immune reactions by cathelicidin. Cathelicidin and IL-36 are engaged, therefore, in the pathogenesis of psoriasis and other skin diseases during the initiation or occasional exacerbation of dermatoses by innate immune stimuli, such as local and general infections and injuries.

Acknowledgments

We thank Yumiko Ito, Natsue Sawaya, and Yuko Yoshida for technical assistance and Momo Miura and Yuko Yanagawa for secretarial support.

Disclosures

The authors have no financial conflicts of interest.

References

1. Schauber, J., R. A. Dorschner, K. Yamasaki, B. Brouha, and R. L. Gallo. 2006. Control of the innate epithelial antimicrobial response is cell-type specific and dependent on relevant microenvironmental stimuli. *Immunology* 118: 509–519.
2. López-García, B., P. H. Lee, K. Yamasaki, and R. L. Gallo. 2005. Anti-fungal activity of cathelicidins and their potential role in *Candida albicans* skin infection. *J. Invest. Dermatol.* 125: 108–115.
3. Howell, M. D., J. F. Jones, K. O. Kisich, J. E. Streib, R. L. Gallo, and D. Y. Leung. 2004. Selective killing of vaccinia virus by LL-37: implications for eczema vaccinatum. *J. Immunol.* 172: 1763–1767.
4. Murakami, M., B. Lopez-Garcia, M. Braff, R. A. Dorschner, and R. L. Gallo. 2004. Postsecretory processing generates multiple cathelicidins for enhanced topical antimicrobial defense. *J. Immunol.* 172: 3070–3077.
5. Yamasaki, K., and R. L. Gallo. 2008. Antimicrobial peptides in human skin disease. *Eur. J. Dermatol.* 18: 11–21.
6. Oppenheim, J. J., and D. Yang. 2005. Alarmins: chemotactic activators of immune responses. *Curr. Opin. Immunol.* 17: 359–365.
7. Morizane, S., K. Yamasaki, B. Mühleisen, P. F. Kotol, M. Murakami, Y. Aoyama, K. Iwatsuki, T. Hata, and R. L. Gallo. 2012. Cathelicidin antimicrobial peptide LL-37 in psoriasis enables keratinocyte reactivity against TLR9 ligands. *J. Invest. Dermatol.* 132: 135–143.
8. Lande, R., J. Gregorio, V. Facchinetti, B. Chatterjee, Y. H. Wang, B. Homey, W. Cao, Y. H. Wang, B. Su, F. O. Nestle, et al. 2007. Plasmacytoid dendritic cells sense self-DNA coupled with antimicrobial peptide. *Nature* 449: 564–569.
9. Kandler, K., R. Shaykhiev, P. Kleemann, F. Klescz, M. Lohoff, C. Vogelmeier, and R. Bals. 2006. The anti-microbial peptide LL-37 inhibits the activation of dendritic cells by TLR ligands. *Int. Immunol.* 18: 1729–1736.
10. Koczulla, R., G. von Degenfeld, C. Kupatt, F. Krötz, S. Zahler, T. Gloe, K. Issbrücker, P. Unterberger, M. Zaiou, C. Lebherz, et al. 2003. An angiogenic role for the human peptide antibiotic LL-37/hCAP-18. *J. Clin. Invest.* 111: 1665–1672.
11. Bromley, S. K., T. R. Mempel, and A. D. Luster. 2008. Orchestrating the orchestrators: chemokines in control of T cell traffic. *Nat. Immunol.* 9: 970–980.
12. Zanetti, M. 2004. Cathelicidins, multifunctional peptides of the innate immunity. *J. Leukoc. Biol.* 75: 39–48.
13. Braff, M. H., M. A. Hawkins, A. Di Nardo, B. Lopez-Garcia, M. D. Howell, C. Wong, K. Lin, J. E. Streib, R. Dorschner, D. Y. Leung, and R. L. Gallo. 2005. Structure-function relationships among human cathelicidin peptides: dissociation of antimicrobial properties from host immunostimulatory activities. *J. Immunol.* 174: 4271–4278.
14. Filewod, N. C., J. Pistolic, and R. E. Hancock. 2009. Low concentrations of LL-37 alter IL-8 production by keratinocytes and bronchial epithelial cells in response to proinflammatory stimuli. *FEMS Immunol. Med. Microbiol.* 56: 233–240.
15. Yu, J., N. Mookherjee, K. Wee, D. M. Bowdish, J. Pistolic, Y. Li, L. Rehaume, and R. E. Hancock. 2007. Host defense peptide LL-37, in synergy with inflammatory mediator IL-1beta, augments immune responses by multiple pathways. *J. Immunol.* 179: 7684–7691.
16. Dorschner, R. A., V. K. Pestonjamasp, S. Tamakuwala, T. Ohtake, J. Rudisill, V. Nizet, B. Agerberth, G. H. Gudmundsson, and R. L. Gallo. 2001. Cutaneous injury induces the release of cathelicidin anti-microbial peptides active against group A *Streptococcus*. *J. Invest. Dermatol.* 117: 91–97.
17. Schauber, J., R. A. Dorschner, A. B. Coda, A. S. Büchau, P. T. Liu, D. Kiken, Y. R. Helfrich, S. Kang, H. Z. Elalieh, A. Steinmeyer, et al. 2007. Injury en-

hances TLR2 function and antimicrobial peptide expression through a vitamin D-dependent mechanism. *J. Clin. Invest.* 117: 803–811.
18. Frohm, M., B. Agerberth, G. Ahangari, M. Stâhle-Bäckdahl, S. Lidén, H. Wigzell, and G. H. Gudmundsson. 1997. The expression of the gene coding for the antibacterial peptide LL-37 is induced in human keratinocytes during inflammatory disorders. *J. Biol. Chem.* 272: 15258–15263.
19. Yamasaki, K., A. Di Nardo, A. Bardan, M. Murakami, T. Ohtake, A. Coda, R. A. Dorschner, C. Bonnart, P. Descargues, A. Hovnanian, et al. 2007. Increased serine protease activity and cathelicidin promotes skin inflammation in rosacea. *Nat. Med.* 13: 975–980.
20. Ong, P. Y., T. Ohtake, C. Brandt, I. Strickland, M. Boguniewicz, T. Ganz, R. L. Gallo, and D. Y. Leung. 2002. Endogenous antimicrobial peptides and skin infections in atopic dermatitis. *N. Engl. J. Med.* 347: 1151–1160.
21. Yamasaki, K., and R. L. Gallo. 2009. The molecular pathology of rosacea. *J. Dermatol. Sci.* 55: 77–81.
22. Saito, R., S. Hirakawa, H. Ohara, M. Yasuda, T. Yamazaki, S. Nishii, and S. Aiba. 2011. Nickel differentially regulates NFAT and NF-κB activation in T cell signaling. *Toxicol. Appl. Pharmacol.* 254: 245–255.
23. Takahashi, T., Y. Kimura, K. Niwa, Y. Ohmiya, T. Fujimura, K. Yamasaki, and S. Aiba. 2013. In vivo imaging demonstrates ATP release from murine keratinocytes and its involvement in cutaneous inflammation after tape stripping. *J. Invest. Dermatol.* 133: 2407–2415.
24. Lai, Y., and R. L. Gallo. 2009. AMPed up immunity: how antimicrobial peptides have multiple roles in immune defense. *Trends Immunol.* 30: 131–141.
25. Jensen, L. E. 2010. Targeting the IL-1 family members in skin inflammation. *Curr. Opin. Investig. Drugs* 11: 1211–1220.
26. Mabuchi, T., T. W. Chang, S. Quinter, and S. T. Hwang. 2012. Chemokine receptors in the pathogenesis and therapy of psoriasis. *J. Dermatol. Sci.* 65: 4–11.
27. Di Cesare, A., P. Di Meglio, and F. O. Nestle. 2009. The IL-23/Th17 axis in the immunopathogenesis of psoriasis. *J. Invest. Dermatol.* 129: 1339–1350.
28. Miller, L. S. 2008. Toll-like receptors in skin. *Adv. Dermatol.* 24: 71–87.
29. Sims, J. E., and D. E. Smith. 2010. The IL-1 family: regulators of immunity. *Nat. Rev. Immunol.* 10: 89–102.
30. Towne, J. E., K. E. Garka, B. R. Renshaw, G. D. Virca, and J. E. Sims. 2004. Interleukin (IL)-1F6, IL-1F8, and IL-1F9 signal through IL-1Rrp2 and IL-1RAcP to activate the pathway leading to NF-kappaB and MAPKs. *J. Biol. Chem.* 279: 13677–13688.
31. Blumberg, H., H. Dinh, E. S. Trueblood, J. Pretorius, D. Kugler, N. Weng, S. T. Kanaly, J. E. Towne, C. R. Willis, M. K. Kuechle, et al. 2007. Opposing activities of two novel members of the IL-1 ligand family regulate skin inflammation. *J. Exp. Med.* 204: 2603–2614.
32. Johnston, A., X. Xing, A. M. Guzman, M. Riblett, C. M. Loyd, N. L. Ward, C. Wohn, E. P. Prens, F. Wang, L. E. Maier, et al. 2011. IL-1F5, -F6, -F8, and -F9: a novel IL-1 family signaling system that is active in psoriasis and promotes keratinocyte antimicrobial peptide expression. *J. Immunol.* 186: 2613–2622.
33. Onoufriadis, A., M. A. Simpson, A. E. Pink, P. Di Meglio, C. H. Smith, V. Pullabhatla, J. Knight, S. L. Spain, F. O. Nestle, A. D. Burden, et al. 2011. Mutations in IL36RN/IL1F5 are associated with the severe episodic inflammatory skin disease known as generalized pustular psoriasis. *Am. J. Hum. Genet.* 89: 432–437.
34. Marrakchi, S., P. Guigue, B. R. Renshaw, A. Puel, X. Y. Pei, S. Fraitag, J. Zribi, E. Bal, C. Cluzeau, M. Chrabieh, et al. 2011. Interleukin-36-receptor antagonist deficiency and generalized pustular psoriasis. *N. Engl. J. Med.* 365: 620–628.
35. Ramadas, R. A., S. L. Ewart, B. D. Medoff, and A. M. LeVine. 2011. Interleukin-1 family member 9 stimulates chemokine production and neutrophil influx in mouse lungs. *Am. J. Respir. Cell Mol. Biol.* 44: 134–145.
36. Chustz, R. T., D. R. Nagarkar, J. A. Poposki, S. Favoreto, Jr., P. C. Avila, R. P. Schleimer, and A. Kato. 2011. Regulation and function of the IL-1 family cytokine IL-1F9 in human bronchial epithelial cells. *Am. J. Respir. Cell Mol. Biol.* 45: 145–153.
37. Milligan, G., J. Lopez-Gimenez, S. Wilson, and J. J. Carrillo. 2004. Selectivity in the oligomerisation of G protein-coupled receptors. *Semin. Cell Dev. Biol.* 15: 263–268.
38. Milligan, G. 2001. Oligomerisation of G-protein-coupled receptors. *J. Cell Sci.* 114: 1265–1271.
39. Takesono, A., M. J. Cismowski, C. Ribas, M. Bernard, P. Chung, S. Hazard III, E. Duzic, and S. M. Lanier. 1999. Receptor-independent activators of heterotrimeric G-protein signaling pathways. *J. Biol. Chem.* 274: 33202–33205.
40. Cismowski, M. J., A. Takesono, M. L. Bernard, E. Duzic, and S. M. Lanier. 2001. Receptor-independent activators of heterotrimeric G-proteins. *Life Sci.* 68: 2301–2308.
41. Sandgren, S., A. Wittrup, F. Cheng, M. Jönsson, E. Eklund, S. Busch, and M. Belting. 2004. The human antimicrobial peptide LL-37 transfers extracellular DNA plasmid to the nuclear compartment of mammalian cells via lipid rafts and proteoglycan-dependent endocytosis. *J. Biol. Chem.* 279: 17951–17956.
42. Sanmiguel, J. C., F. Olaru, J. Li, E. Mohr, and L. E. Jensen. 2009. Interleukin-1 regulates keratinocyte expression of T cell targeting chemokines through interleukin-1 receptor associated kinase-1 (IRAK1) dependent and independent pathways. *Cell. Signal.* 21: 685–694.
43. Ohta, Y., Y. Hamada, and K. Katsuoka. 2001. Expression of IL-18 in psoriasis. *Arch. Dermatol. Res.* 293: 334–342.
44. Carrier, Y., H. L. Ma, H. E. Ramon, L. Napierata, C. Small, M. O'Toole, D. A. Young, L. A. Fouser, C. Nickerson-Nutter, M. Collins, et al. 2011. Inter-regulation of Th17 cytokines and the IL-36 cytokines in vitro and in vivo: implications in psoriasis pathogenesis. *J. Invest. Dermatol.* 131: 2428–2437.

STEM CELLS AND DEVELOPMENT
Volume 23, Number 7, 2014

DOI: 10.1089/scd.2013.0473

Human Adipose Tissue Possesses a Unique Population of Pluripotent Stem Cells with Nontumorigenic and Low Telomerase Activities: Potential Implications in Regenerative Medicine

Fumitaka Ogura,[1] Shohei Wakao,[1] Yasumasa Kuroda,[2] Kenichiro Tsuchiyama,[1,3] Mozhdeh Bagheri,[1] Saleh Heneidi,[4] Gregorio Chazenbalk,[5] Setsuya Aiba,[3] and Mari Dezawa[1,2]

Abstract

In this study, we demonstrate that a small population of pluripotent stem cells, termed adipose multilineage-differentiating stress-enduring (adipose-Muse) cells, exist in adult human adipose tissue and adipose-derived mesenchymal stem cells (adipose-MSCs). They can be identified as cells positive for both MSC markers (CD105 and CD90) and human pluripotent stem cell marker SSEA-3. They intrinsically retain lineage plasticity and the ability to self-renew. They spontaneously generate cells representative of all three germ layers from a single cell and successfully differentiate into targeted cells by cytokine induction. Cells other than adipose-Muse cells exist in adipose-MSCs, however, do not exhibit these properties and are unable to cross the boundaries from mesodermal to ectodermal or endodermal lineages even under cytokine inductions. Importantly, adipose-Muse cells demonstrate low telomerase activity and transplants do not promote teratogenesis in vivo. When compared with bone marrow (BM)– and dermal-Muse cells, adipose-Muse cells have the tendency to exhibit higher expression in mesodermal lineage markers, while BM- and dermal-Muse cells were generally higher in those of ectodermal and endodermal lineages. Adipose-Muse cells distinguish themselves as both easily obtainable and versatile in their capacity for differentiation, while low telomerase activity and lack of teratoma formation make these cells a practical cell source for potential stem cell therapies. Further, they will promote the effectiveness of currently performed adipose-MSC transplantation, particularly for ectodermal and endodermal tissues where transplanted cells need to differentiate across the lineage from mesodermal to ectodermal or endodermal in order to replenish lost cells for tissue repair.

Introduction

MESENCHYMAL STEM CELLS (MSCs) derived from adipose tissue are multipotent stromal cells that can differentiate into adipocytes, chondrocytes, osteoblasts, and myoblasts in vitro and undergo differentiation in vivo [1]. MSCs are currently being applied in a number of clinical studies that target numerous diseases because of their accessibility, nontumorigenicity, and powerful trophic effects [2,3].

MSCs derived from adipose tissue (adipose-MSCs) provide an abundant and minimally invasive source of cells [4]. Adipose-MSCs can be maintained in culture for extended periods of time and can be induced in vitro to differentiate into all mesenchymal cell lineages [1,4]. Moreover, adipose-MSCs can be safely and efficiently transplanted to autologous hosts, and they are currently being used successfully for a variety of regenerative therapies [2,3].

Although not in high ratio, adipose-MSCs also have the capacity to differentiate into neuronal cells [5,6], Schwann cells [7], beta cells [8], and hepatocytes [9,10] in the presence of specific cell differentiation media. Thus adipose-MSCs may cross the oligolineage boundaries from mesodermal to ectodermal or endodermal lineages. Adipose-MSCs exhibit

Departments of [1]Stem Cell Biology and Histology, [2]Anatomy and Anthropology, and [3]Dermatology, Tohoku University Graduate School of Medicine, Sendai, Japan.
[4]Medical College of Georgia, Georgia Regents University, Augusta, Georgia.
[5]Department of Obstetrics and Gynecology, David Geffen School of Medicine at University of California Los Angeles, Los Angeles, California.

a wide variety of triploblastic differentiation not only in vitro, but also in vivo. At a low ratio, they may spontaneously differentiate into hepatocyte-marker-positive cells in the damaged liver [11,12], neuronal- and glial-marker-positive cells in ischemic brain injury [13,14], and cardiomyocytes in acute myocardial infarction [15] after homing to damaged sites. The low rate of adipose-MSC differentiation into ectodermal and endodermal cell lineages could be explained in part by the presence of a small population of stem cells within the adipose-MSC population that have the ability to differentiate to any type of cells, much like pluripotent stem cells. Isolation of such stem cells could have a critical impact in regenerative medicine and cell therapy.

Recently, a novel population of stem cells with pluripotent characteristics has been isolated from mesenchymal tissues, such as human skin fibroblasts and bone marrow (BM). These cells, termed multilineage-differentiating stress-enduring (Muse) cells, are of mesenchymal origin, comprise several percentages of human dermal fibroblasts and BM-MSCs, and are highly resistant to cellular stress. They are double positive for CD105, an MSC marker, and the stage-specific embryonic antigen-3 marker (SSEA-3), well known for the characterization of undifferentiated human embryonic stem (ES) cells. Muse cells can differentiate into cells of ectodermal, endodermal, and mesodermal lineages both in vitro and in vivo, and have the ability to self-renew [16]. Advantageously, Muse cells do not produce teratomas in vivo, nor do they induce immunorejection in the host upon autologous transplantation [16,17]. In addition, Muse cells are shown to home into the damaged site in vivo and spontaneously differentiate into tissue-specific cells according to the microenvironment to contribute to tissue regeneration when infused into the blood stream [16].

In the present study, we isolated Muse cells derived from human adipose tissue (adipose-Muse cells) using SSEA-3-cell-sorting techniques. Further characterization indicates that SSEA-3(+) adipose-Muse cells express general mesenchymal markers CD105, CD90, and CD29 [18,19]. They express the pluripotent stem cell markers Nanog, Oct3/4, PAR4, Sox2, and TRA-1-81 and can spontaneously differentiate into cells representative of all three germ layers from a single cell. Conversely, alternate cells in adipose-MSCs, SSEA-3 (−) adipose-MSCs (adipose-non-Muse cells), can only differentiate into mesenchymal but not into ectodermal and endodermal cell lineages even under the presence of cytokine induction. Further, adipose-Muse cells are negative for CD34 and CD146, known as classical adipose-derived stem cell (ADSC) markers [4]. While core properties of Muse cells among BM, dermis, and adipose tissues, namely, triploblastic differentiation, self-renewal, and non-tumorigenicity, are the same, BM- and dermal-Muse cells show higher expression of ectodermal and endodermal lineage markers while adipose-Muse cells show a tendency for higher expression of mesodermal markers, and preferentially differentiate into mesodermal cell lineages, suggesting that the propensity for differentiation is in accordance with the source of tissue from which Muse cells are derived.

In contrast to ES and induced pluripotent stem (iPS) cells, adipose-Muse cells have low telomerase activity and do not produce teratomas in vivo, which may alleviate one of the primary concerns with the use of pluripotent stem cells in the clinical arena. Adipose-Muse cells could be an ideal source of pluripotent stem cells with the potential to have a critical impact on regenerative medicine.

Materials and Methods

Cell source

Two different sources of adipose-MSCs were used in this study: adipose-MSCs commercially purchased from Lonza (LA-MSCs) and freshly isolated adipose-MSCs from subcutaneous adipose tissue (AT-MSCs). Cells were maintained at 37°C in Dulbecco's modified Eagle's medium high-glucose (DMEM; Gibco) containing 15% fetal bovine serum (FBS) and 0.1 mg/mL kanamycin sulfate (Gibco) in an atmosphere containing 5% CO_2.

The use of human subcutaneous adipose tissue was approved by the Ethics Committee for Animal Experiments at the Tohoku University Graduate School of Medicine. Subcutaneous adipose tissue was provided by Department of Dermatology, Tohoku University Graduate School of Medicine with informed consent. Isolation of AT-MSCs from adipose tissue was done according to the method previously reported by Estes et al. with minor modification [20]. In brief, adipose tissue was minced into small pieces and incubated in equal volume of phosphate-buffered saline (PBS, without calcium chloride and magnesium chloride) containing 1 mg/mL Collagenase Type I (Worthington Biochemical) and 1% bovine serum albumin (Nacalai) at 37°C for 1 h with mild shaking. Digested material was then centrifuged at 300 *g* for 5 min to obtain a cell pellet. The pellet was resuspended and filtered through a 100-μm nylon mesh filter (Becton Dickinson) and centrifuged again at 300 *g* for 5 min. The pellet was resuspended in DMEM containing 15% FBS and 0.1 mg/mL kanamycin sulfate and cultured. Cells were plated in adherent dishes at density of 3.5×10^4 cells/cm^2 and cultured after reaching ~90% confluence, exhibiting a fibroblast-like shape. The doubling time of the cells was 0.9–1.3 days/cell division.

Mouse ES cells (TT2 cells) were cultured at 37°C in DMEM containing 15% FBS, 0.1 mg/mL kanamycin sulfate, 0.1 mM MEM non-essential amino acid solution (NEAA; Gibco), 1 mM sodium pyruvate solution (SP; Gibco), 1000 U/mL leukemia inhibitory factor (Merk), and 100 μM 2β-mercaptoethanol on mitomycin-C-treated mouse embryonic fibroblast feeder cells established from 12.5-day embryos of C57BL/6 mice.

Fluorescence-activated cell sorting

Confluent adipose-MSCs (two to eight passages) were used for cell sorting. Cells were collected by trypsin-EDTA (0.25%) treatment, centrifuged, and resuspended in fluorescence-activated cell sorting (FACS) buffer (PBS containing 0.5% BSA and 2 mM EDTA) [21] at a concentration of 1×10^6 cells/100 μL. Cells were incubated in FACS buffer containing 15% human serum for 20 min. After two successive washes by FACS buffer, cells were incubated with anti-SSEA-3 antibody (1:50; Millipore) for 1 h at 4°C. Cells were then washed three times with FACS buffer, followed by FITC-conjugated anti-rat IgM (1:100; Jackson ImmunoResearch) for 1 h at 4°C. After three consecutive washes in FACS buffer, cells were sorted for SSEA-3(+) and SSEA-3(−) cells (adipose-Muse and -non-Muse cells)

by Special Order Research Products FACSAriaII (Becton Dickinson) using a low stream speed. This ensured a high level of cell survival and the highest purity of the sorted cells, via the four-way purity sorting mode, as previously described [21]. SSEA-3(+)-adipose-Muse cells (labeled with FITC) were analyzed by flow cytometry for the expression of cell surface antigens CD29 [labeled with phycoerythrin (PE)], CD90 (PE), CD105 (Pacific Blue), CD34 (PE), and CD146 (PE) (Becton Dickinson).

Single-cell suspension culture

Adipose-Muse cells were cultured as floating cells using poly-HEMA-coated dishes as previously described [21]. Each single cell was plated in an individual well on 96-well plates after limiting dilution with alpha-MEM medium containing 15% FBS. The actual number of cells deposited in each well was determined by visual inspection using a phase-contrast microscope, and empty wells or wells with more than one cell were excluded from analysis.

Spontaneous differentiation of clusters in vitro

After 7–10 days of single-cell suspension culture, single clusters of adipose-Muse cells were picked up with a glass micropipette and transferred onto a gelatin-coated culture dish or cover glass. After another 7–10 days of incubation, clusters were subjected to immunocytochemistry and reverse-transcription polymerase chain reaction (RT-PCR).

Immunocytochemistry

Immunocytochemistry was performed as previously described [21]. Clusters of adipose-Muse cells were fixed with 4% paraformaldehyde in 0.01 M PBS, embedded in OCT compound, and then cut into 8-μm-thick cryosections. Differentiated cells derived from adipose-Muse cell cluster were grown in gelatin-coated dishes. Cells were fixed using the same fixative described earlier. Antibodies used in this study included Nanog (1:100; Millipore), Oct3/4 (1:100; Santa Cruz Biotechnology), Sox2 (1:1000; Millipore), PAR4 (1:100; Santa Cruz Biotechnology), TRA-1-81 (1:100; Santa Cruz Biotechnology), smooth muscle actin (SMA, 1:100; Lab Vision, Thermo Fisher Scientific), neurofilament-M (1:100; Millipore), cytokeratin 7 (CK7, 1:100; Millipore), alpha-fetoprotein (α-FP, 1:100; DAKO), fatty acid-binding protein 4 (FABP-4, 1:100; R&D Systems), human hepatocyte paraffin-1 (HepPar1, 1:200; Dako), delta-like protein-1 (DLK1, 1:100; Santa Cruz), human albumin (1:100; Bethyl Laboratories), and neuronal class III β-tubulin (Tuj-1, 1:1000; Covance). All primary antibodies were diluted 1:200 in PBS/0.1% BSA solution and incubated overnight at 4°C. Following treatment with primary antibodies, cells were washed three times with PBS and incubated for 1 h at R/T with PBS/0.1% BSA containing secondary immunofluorescent antibodies. These antibodies included FITC-, Alexa-488-, or Alexa-568-labeled conjugated anti-rabbit IgG, anti-mouse IgG, anti-mouse IgM, or anti-rat IgM (1:100; Jackson ImmunoResearch). Nuclei were identified by 4′,6-diamidino-2-phenylindole (DAPI) staining (1:1000; Sigma). Cells were then washed three times with PBS. Images were acquired with a confocal laser scanning microscope (CS-1; Nikon).

RT-PCR

Total RNA was extracted from cells and purified using NucleoSpin RNA XS (Macherey-Nagel). First-strand cDNA was generated using the SuperScript VILO cDNA Synthesis Kit (Invitrogen) according to the manufacturer's instructions. The PCRs were performed using Ex Taq DNA polymerase using standard temperature cycling conditions (TaKaRa Bio). The primers used were (1) β-actin sense 5′-AGGCGGACTATGACTTAGTTGCGTTACACC-3′ and antisense 5′-AAGTCCTCGGCCACATTGTGAACTTTG-3′, (2) Nkx2.5 sense 5′-GGGACTTGAATGCGGTTCAG-3′ and antisense 5′-CTCCACAGTTGGGTTCATCTGTAA-3′, (3) α-FP sense 5′-CCACTTGTTGCCAACTCAGTGA-3′ and antisense 5′-TGCAGGAGGGACATATGTTTCA-3′; (4) microtubule associated protein-2 (MAP-2) sense 5′-ACTACC AGTTTCACACCCCCTTT-3′ and antisense 5′-AAGGGT GCAGGAGACACAGATAC-3′, and (5) GATA6 sense 5′-CCTGCGGGCTCTACAGCAAGATGAAC-3′ and antisense 5′-CGCCCCTGAGGCTGTAGGTTGTGTT-3′.

Evaluation for cell self-renewal

Cell self-renewal of adipose-Muse cell clusters was performed as previously described [21]. Briefly, adipose-Muse cells isolated by FACS were grown in single-cell suspension after limiting dilution to generate the first-generation cluster. After 7–10 days of single-cell suspension culture, first-generation clusters were transferred onto an adherent culture for expansion. After another 7 days of incubation of first-generation clusters in adherent culture, expanded cells were collected by trypsinization and returned to single-cell suspension culture after limiting dilution to form second-generation cluster. This cycle was repeated up to third-generation clusters. In each generation step, samples were subjected to RT-PCR.

Test for teratoma formation in immune-deficient mice testes

Adipose-Muse cells (1×10^5 cells) were suspended in PBS and injected using glass micropipette into the testes of 8-week-old CB17/Icr-Prkdc scid/CrlCrlj(SCID) mice ($n=6$). Mice were sacrificed for analysis 6 months after injection. For negative control, testes were injected with PBS ($n=2$) and, for positive control, 5×10^5 mouse ES cells ($n=4$) were injected, and were sacrificed 8 weeks after injection. Tissues were fixed with 4% paraformaldehyde in 0.01 M PBS and 3-μm-thick paraffin sections and analyzed by HE staining.

Telomerase activity

Telomerase activity was detected using TRAPEZE XL telomerase detection kit (Millipore) and Ex Taq polymerase (TaKaRa Bio). Fluorescence intensity was measured with a microplate reader (infinite M1000; Tecan) as described by Wakao et al. [17].

In vitro differentiation into adipocytes, hepatocytes, and neuronal cells

Experiments were repeated three times for each differentiation. Adipose-Muse cells and -non-Muse cells were

incubated in adipogenic differentiation medium (R&D Systems) for 14 days. Formation of new adipocytes was detected using the human MSC functional identification kit (R&D Systems) [19]. For hepatocyte induction, adipose-Muse cells (at a density of 2.0×10^4 cells/cm^2) were cultured on collagen-coated dishes for 14 days in DMEM supplemented with 10% FBS, insulin-transferrin-selenium (Gibco), 10 nM dexamethasone (Sigma), 100 ng/mL hepatocyte growth factor (R&D Systems), and 50 ng/mL fibroblast growth factor-4 (R&D Systems) [9]. Neuronal differentiation was performed according to the method reported by Boulland et al. [6]. Briefly, cells were induced by culture in the Neurobasal medium (Invitrogen) containing 1% FCS, 1×B27 supplement, 0.5 mM 1-methyl-3 isobutylxanthine, 1 mM dexamethasone, 0.2 mM 8CPTcAMP, 10 mM valproic acid, and 10 mM forskolin for 7 days. Comparatively, adipose-non-Muse, SSEA-3 (−) cells obtained from the same adipose tissue were used as controls in all these cell differentiation studies.

Quantitative PCR (q-PCR)

Adipose-Muse cells were induced to neuronal differentiation and total RNA was extracted as described previously. Customized primers for Tuj-1 were purchased from SA Biosciences. Total RNA of BM- (Lonza) and dermal-Muse cells (Lonza) and adipose-Muse cells from LA-MSCs was collected using the RNeasy Mini Kit (Qiagen), and cDNA was synthesized using the RT2First Strand Kit (SA Biosciences). In both experiments, DNA was amplified with the Applied Biosystems 7300 real-time PCR system according to the manufacturer's instructions. Data were processed using the ΔΔCT method [22].

Comparative analysis of gene expression

Total RNA of Muse cells derived from BM (Lonza), normal human dermal fibroblasts (Lonza), and LA-MSCs was extracted and purified using NucleoSpin RNA XS (TaKaRa Bio). The poly-A RNA molecules were further purified from total RNA using poly-T oligo-attached magnetic beads, and then fragmented and converted into cDNA using Illumina TruSeq RNA Sample Prep Kit (Illumina) to make libraries. The quality of libraries was determined with Agilent 2100 Bioanalyzer. The libraries were analyzed by Illumina HiSeq2000 sequencing (Illumina) according to standard procedure. Paired-end 100-bp reads were generated and subjected to data analysis with the use of the platform provided by DNAnexus.

Results

Culture of adipose-MSCs

This study utilized two sources of human adipose-MSCs; five lots of commercially available LA-MSCs that are widely used as adipose-derived MSCs, and four lots of adipose-MSCs established from human subcutaneous adipose tissue, namely, AT-MSCs. For AT-MSCs, volumes, culture duration, and total number of MSCs obtained from the four samples are shown in Supplementary Fig. S1 (Supplementary Data are available online at www.liebertpub.com/scd). On average, a culture of 15 cm^3 of adipose tissue for 3 weeks yielded $\sim 3 \times 10^7$ adipose-MSCs. There were no significant differences observed in morphology or doubling time between LA-MSCs and AT-MSCs (Supplementary Fig. S1).

Characterization of adipose-Muse cells in LA-MSCs and AT-MSCs

We previously reported the presence of Muse cells in the adult human BM and dermis isolated by cell sorting using SSEA-3, a pluripotent stem cell marker for undifferentiated ES cells [16,17]. FACS analysis revealed the presence of SSEA-3-positive cells in LA-MSCs (3.8% ± 0.9%) and AT-MSCs (8.8 ± 1.3), which are termed as adipose-Muse cells in the following descriptions (Fig. 1A, B and Supplementary Table S1).

Surface marker expression was further analyzed in these adipose-Muse cells. They expressed general mesenchymal markers; all of SSEA-3(+)-adipose-Muse cells expressed CD105 (100%) and CD90 (100%), and in a lesser ratio (60%–70%) with CD29 (Fig. E–H). Adipose tissue is generally known to contain so-called ADSCs that express both CD34 and CD146 markers [23]. Adipose-Muse cells isolated from both LA-MSCs and AT-MSCs were, however, negative for these markers, suggesting that they are a distinct population from ADSCs (Fig. 1I, J).

When adipose-Muse cells were transferred to a single-cell suspension culture, each cell began to proliferate and form a cluster that is similar to the human-ES-cell-derived embryoid body formed in suspension culture at days 7–10 (Fig. 1C, D). On an average, adipose-Muse cells derived from LA-MSCs and AT-MSCs formed clusters in a single-cell suspension at a ratio of 31.3% ± 2.8% and 40.9% ± 6.8%, respectively (Supplementary Table S1). Importantly, none of the SSEA-3 (−) adipose-MSCs, namely, adipose-non-Muse cells, obtained from both LA-MSCs and AT-MSCS formed clusters in a single-cell suspension.

Adipose-Muse cell clusters both from LA-MSCs and AT-MSCs expressed pluripotency markers Nanog, Oct3/4, PAR4, Sox2, and TRA-1-81 and were positive for alkaline phosphatase reaction, one of the indicators of ES cells (Fig. 2). When these single-cell-derived clusters were individually transferred onto gelatin-coated dish and cultured adherently for 10–14 days, cells expanded from the cluster and proliferated. Among the expanded cell population, cells positive for α-FP (endodermal marker), SMA (mesodermal), and neurofilament (ectodermal) were recognized (Fig. 3A–D). Cells expanded from clusters of adipose-Muse cells were collected and analyzed by RT-PCR, and gene expression was detected for *NKX2-5* (mesodermal), *GATA6* (endodermal), *MAP2* (ectodermal), and *α-FP* (endodermal) (Fig. 3E). Expression of these genes further indicated that adipose-Muse cells, from either LA-MSCs or AT-MSCs, may have the ability to spontaneously generate cells representative of all three germ layers from a single cell.

To examine the potential for self-renewal, adipose-Muse cells from LA-MSCs and AT-MSCs were subjected to single-cell suspension culture in order to obtain first-generation clusters. Half of the clusters were transferred individually onto gelatin culture, maintained, and analyzed by RT-PCR for the expression of endodermal, mesodermal, and ectodermal markers, as described previously. The rest of the

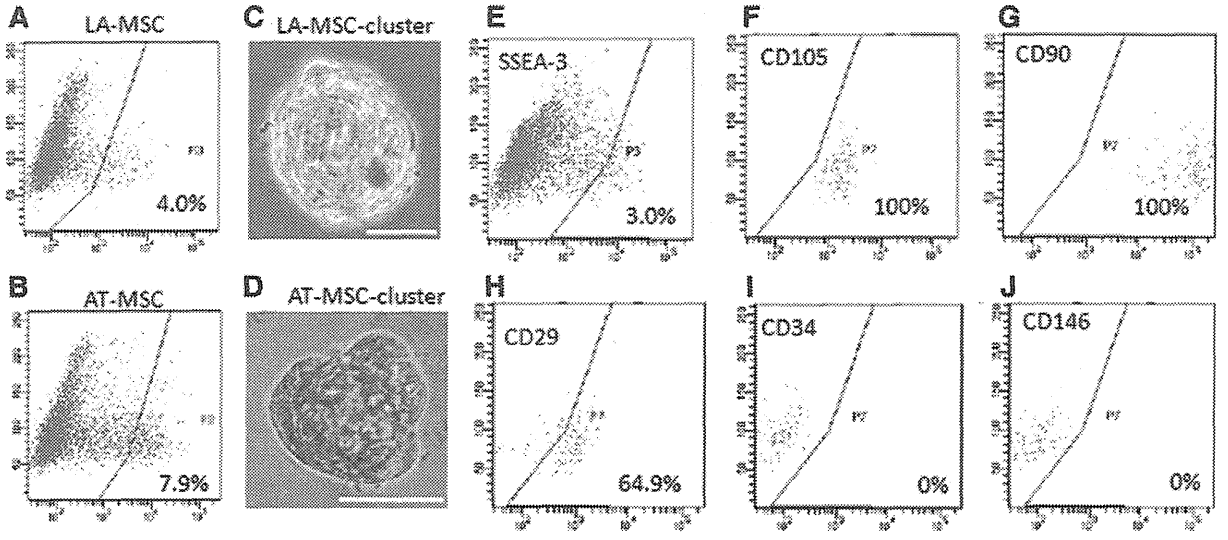

FIG. 1. Characterization of SSEA-3(+) cells in LA-MSCs and AT-MSCs. **(A, B)** An example of SSEA-3(+) cells in LA-MSC **(A)** and AT-MSC **(B)** FACS analysis showed the presence of SSEA-3(+) cells in both populations. **(C, D)** Clusters were formed in single-cell suspension culture from LA-MSC- **(C)** and AT-MSC-SSEA-3(+) cells **(D)**. Scale bars = 50 μm. **(E–J)** Expression of mesenchymal and ADSC markers in LA-MSC-SSEA-3(+) cells. Cells positive for SSEA-3 **(E)** were positive for CD105 **(F)**, CD90 **(G)**, and CD29 **(H)** but were negative for CD34 **(I)** and CD146 **(I)**. AT-MSCs, adipose-MSCs from subcutaneous adipose tissue; LA-MSCs, adipose-MSCs commercially purchased from Lonza. Color images available online at www.liebertpub.com/scd

clusters were individually transferred to adherent culture and allowed to proliferate for 7–10 days, after which they underwent a second round of single-cell suspension in culture to generate second-generation clusters (Fig. 4). This experimental cycle was repeated three times and clusters from each step were analyzed by RT-PCR. Again, gene expression of *MAP2*, *GATA6*, *α-FP*, and *NKX2.5* was detected in first-, second-, and third-generation clusters, demonstrating that adipose-Muse cells maintain self-renewal as well as triploblastic differentiation ability up to the third generation (Fig. 4).

Telomerase activity and in vivo transplantation of adipose-Muse cells

Being a strong indicator of tumorigenicity, telomerase activity was examined in adipose-Muse cells from LA-MSCs and AT-MSCs. High telomerase activity was observed

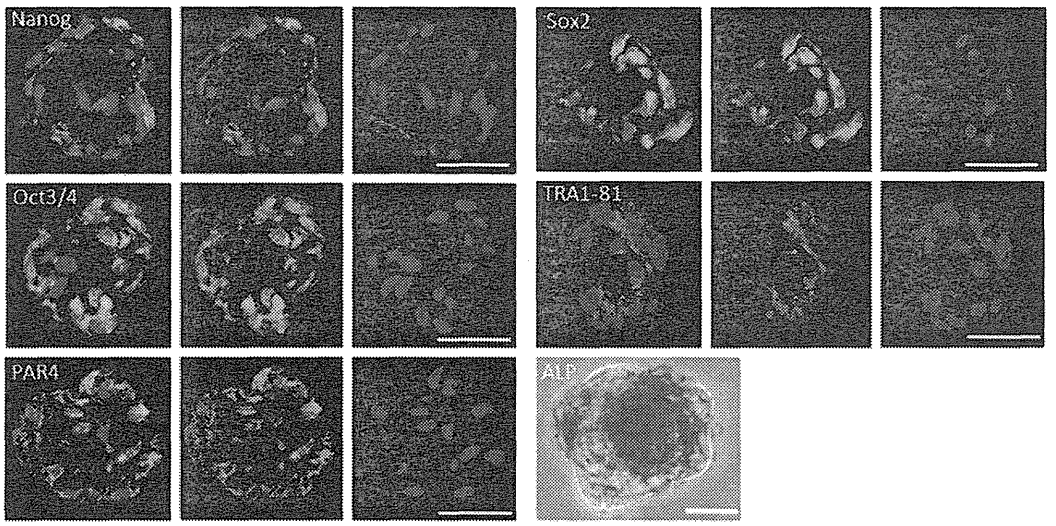

FIG. 2. Immunostaining of clusters formed from adipose-Muse cells in single-cell suspension culture. Clusters were positive for Nanog, Oct3/4, PAR4, Sox2, and TRA1-81, as well as for reactive alkaline phosphatase (ALP). Nanog, Oct3/4, and TRA-1-81 were from AT-MSC-SSEA-3(+) cells and PAR4, Sox2, and ALP from LA-MSC-SSEA-3(+) cells. Scale bars = 25 μm. Color images available online at www.liebertpub.com/scd

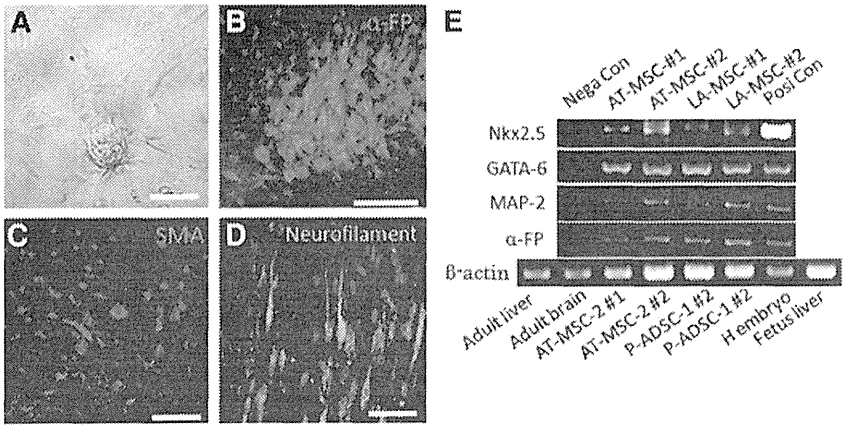

FIG. 3. Differentiation of single-Muse-cell-derived cluster into endodermal, mesodermal, and ectodermal lineages. Clusters formed from adipose-Muse cells of LA-MSCs in single-cell suspension culture were transferred onto gelatin-coated culture **(A)** allowing the cells to expand and differentiate spontaneously, expressing alpha-fetoprotein (α-FP: endodermal) **(B)**, smooth muscle actin (SMA: mesodermal) **(C)**, and neurofilament (ectodermal) **(D)**. Scale bars = 100 μm. RT-PCR analysis of cells expanded from single adipose-Muse cell cluster detected signals for *Nkx2.5* (mesodermal), *GATA-6* (endodermal), *MAP-2* (ectodermal), and *α-FP* (endodermal) in both AT-MSCs and LA-MSCs **(E)**. Positive controls for *Nkx2.5, MAP-2,* and *α-FP* were human whole embryo (H embryo) and for *GATA-4* was human fetus liver (Fetus liver). Negative controls for *Nkx2.5* and *MAP-2* were human adult liver (Adult liver) and for *GATA-6* and *α-FP* were human adult brain (Adult brain). RT-PCR, reverse transcription-polymerase chain reaction. Color images available online at www.liebertpub.com/scd

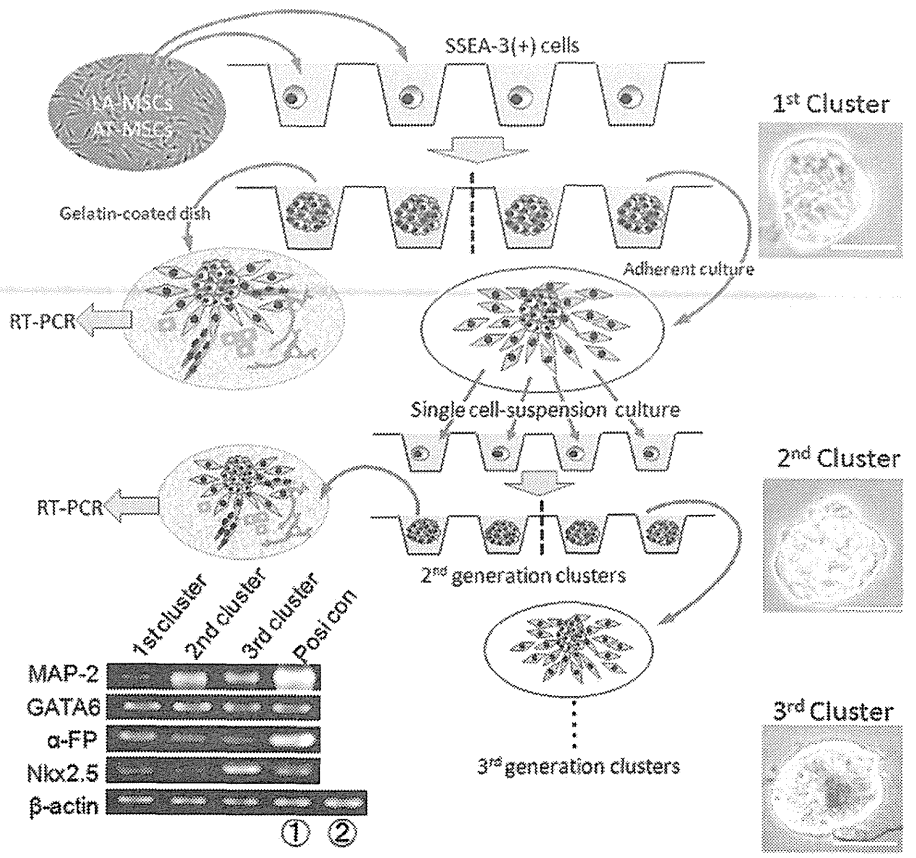

FIG. 4. Adipose-Muse cells demonstrate the capacity for self-renewal. Schematic diagram outlines experiments that validate self-renewal ability of adipose-Muse cells. RT-PCR data are from AT-MSC-derived adipose-Muse cells as an example. *MAP-2* (ectodermal), *GATA-6* (endodermal), *α-FP* (endodermal), and *Nkx2.5* (mesodermal) gene expression was detected in RT-PCR from cells expanded from each of clusters from first to third generations. Adipose-Muse cells from LA-MSCs showed basically same data (not shown). Positive controls for *MAP-2, α-FP,* and *Nkx2.5* were human whole embryo and for *GATA-4* was human fetus liver. 1 and 2 in *β-actin* are from human whole embryo (1) and human fetus liver (2), respectively. Scale bars = 25 μm. Color images available online at www.liebertpub.com/scd

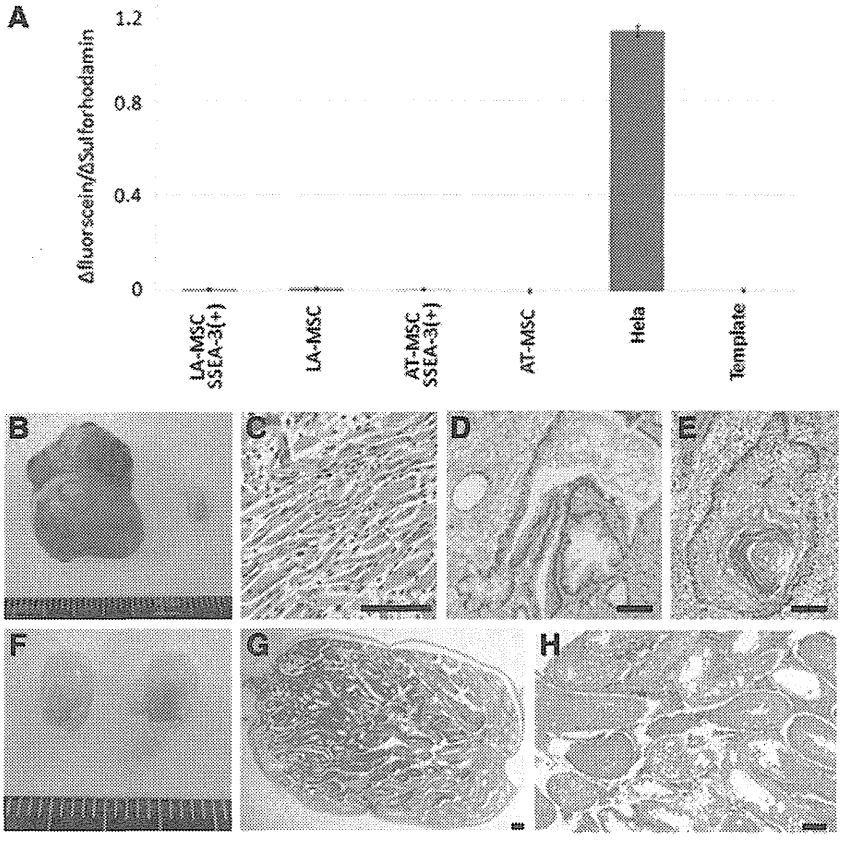

FIG. 5. Nontumorigenicity of adipose-Muse cells. **(A)** Telomerase activity in LA-MSCs, AT-MSCs, as well as adipose-Muse cells [SSEA-3(+)] from both populations. Hela cells (Hela) were used as positive control and template for negative control. **(B–E)** Teratoma formation in mouse testis with mouse ES cell transplantation (8 weeks after) **(B)**. Histological analysis showed that the teratoma contained muscle tissue **(C)**, intestine-like structure **(D)**, and keratinized skin formation **(E)**. **(F–H)** Transplantation of adipose-Muse cells from LA-MSCs into Nog mouse testis did not form teratoma even after 6 months **(F)** and maintained normal testis structure **(G, H)**. Scale bars = 100 μm. Color images available online at www.liebertpub.com/scd

in Hela cells, while adipose-Muse cells both from LA-MSCs and AT-MSCs were at nearly the same reduced level as cells from the original LA-MSC and AT-MSC populations (Fig. 5A).

Next, cell transplantation was performed in the testes of immune-deficient mice. When mouse ES cells were transplanted, large teratomas, consisting of mesodermal, endodermal, and ectodermal tissues, were formed by 8–10 weeks (Fig. 5B–E), while even after 6 months, the adipose-Muse cells transplanted in the mouse testes never formed teratomas. Normal testicular tubes were maintained in these testes (Fig. 5F–H).

All of the characteristics present in adipose-Muse cells, namely, expression both of pluripotency and mesenchymal markers, generation of embryoid-body-like clusters in suspension, triploblastic differentiation from a single cell, self-renewal, and nontumorigenicity, were consistent with previously reported BM- and dermal-Muse cells [16,17,21].

Cytokine induction into endodermal, ectodermal, and mesodermal lineages

Adipose-Muse and -non-Muse cells were treated with cocktails of cytokines and reagents for adipocyte (mesodermal), hepatocyte (endodermal), and neuronal cell (ectodermal) differentiation. In adipocyte induction, both adipose-Muse and -non-Muse cells generated cells with lipid droplets that were positive for Oil Red-O staining. Immunolabeling of FABP-4, however, resulted in 72.4% ± 3.4% of adipose-Muse cells that display positivity, while adipose-non-Muse cells were only 34.4% ± 2.9% positive, suggesting that adipose-Muse cells have higher potential to become adipocytes than adipose-non-Muse cells (Fig. 6A–D).

Hepatocyte induction demonstrated that cells positive for hepatic stem cell marker human DLK1, and hepatocyte markers human HepPar1 and human albumin were induced from adipose-Muse cells but not from adipose-non-Muse cells. The positivity for human albumin in adipose-Muse cells was 13.7% ± 1.6% while it was undetectable in adipose-non-Muse cells (Fig. 6E–H).

Neuronal induction in adipose-Muse cells resulted in generation of cells positive for Tuj-1 with neuron-like morphology. These cells were generated from adipose-Muse cells but not from adipose-non-Muse cells. These results were also confirmed by q-PCR of Tuj-1 expression (Fig. 6I–M).

These results suggest that both adipose-Muse and -non-Muse cells are capable of differentiating into mesodermal lineage cells, such as adipocytes; however, higher efficiency is anticipated in adipose-Muse cells rather than -non-Muse cells. In contrast, differentiation from mesodermal to ectodermal or endodermal lineages was only possible in adipose-Muse cells.

Comparison among BM-, dermal-, and adipose-Muse cells

Muse cells collected as SSEA-3(+) cells from human BM-MSCs (BM-Muse), dermal fibroblasts (dermal-Muse),

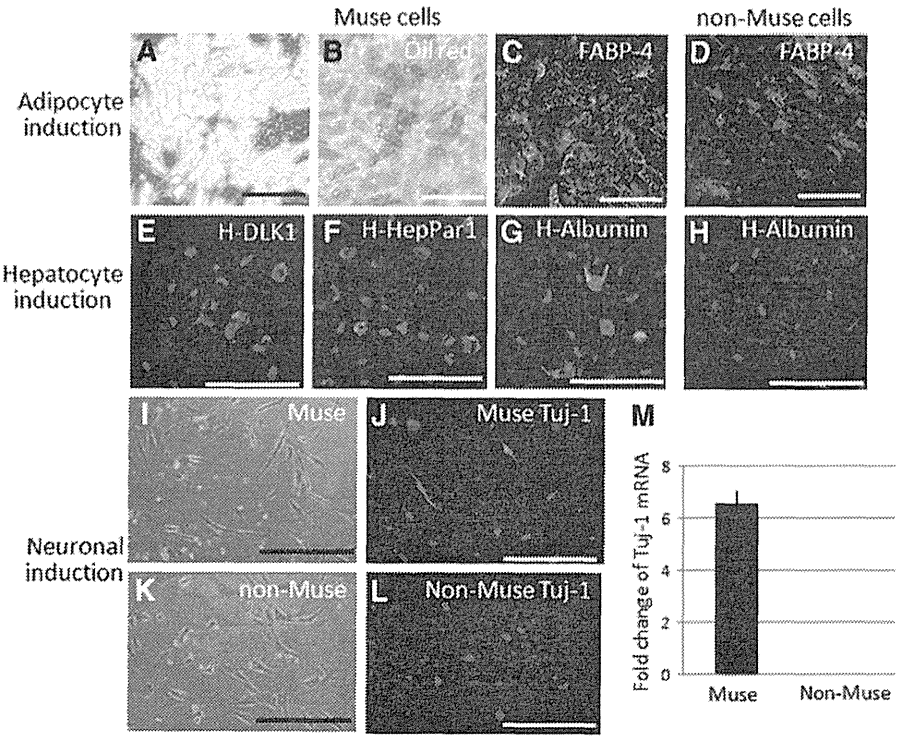

FIG. 6. Induced differentiation of adipose-Muse and -non-Muse cells. (**A–D**) Muse (**A–C**) and non-Muse (**D**) cells from LA-MSCs were subjected to adipocyte induction. Cells with lipid droplets (**A**) that are stained with Oil Red-O (**B**) were detected in adipose-Muse cells. Those cells were also positive for the adipocyte marker FABP-4. Adipose-non-Muse cells also contained cells positive for FABP-4 but with lower ratio (**D**). (**E–H**) After hepatocyte induction, Muse cells were positive for liver stem cell marker human-DLK1 (**E**) and hepatocyte markers human HepPar1 (**F**) and human albumin (**G**), while non-Muse cells lacked these expression. An example of non-Muse cells was shown in human albumin expression (**H**). (**I–M**) After neuronal induction, Muse cells demonstrated a morphology similar to neuronal cells (**I**), and some were also positive for Tuj-1 (**J**). However, adipose-non-Muse cells were not like neuronal cells (**K**) and all cells were Tuj-1 negative (**L**). Q-PCR consistently detected *Tuj-1* signal only in Muse cells and not in non-Muse cells (**M**). Scale bars = 100 μm. Color images available online at www.liebertpub.com/scd

and LA-MSCs (adipose-Muse) were subjected to next generation sequencing to compare expression levels of genes related to endodermal, mesodermal, and ectodermal differentiation (Table 1). Analysis of mesodermal lineage expression revealed that osteogenic, adipogenic, and myogenic genes were generally higher in adipose-Muse rather than BM-Muse or dermal-Muse cells, and some of the factors, such as SP7, osteogenic factor, and Pax7 muscle stem cell marker, were only detected in adipose-Muse cells. Different from mesodermal factors, endodermal factors were more predominantly expressed in BM-Muse cells than in adipose-Muse cells. However, cholesterol 7, alpha-hydroxylase (CYP7A1), insulin gene enhancer binding protein (ISL1), and hepatocyte nuclear factor 4 alpha (HNF4A) were only expressed in adipose-Muse cells and not in BM-Muse or dermal-Muse cells (Table 1). Ectodermal genes that relate to neuronal differentiation were higher in both BM-Muse and dermal-Muse cells than in adipose-Muse cells while factors such as genes encoding for musashi RNA-binding protein 1 (MSI1), ISL1, and myelin transcription factor 1-like (MYT1L) were not expressed in BM-Muse or dermal-Muse cells, but only in adipose-Muse cells (Table 1).

Discussion

In this study, we demonstrate that both adult human subcutaneous adipose tissue and commercially available adipose-MSCs contain a small percentage of stem cells with the capacity for triploblastic differentiation and self-renewal. These cells do not undergo tumorigenic proliferation in vitro, nor do they elicit teratomas when transplanted in vivo. These characteristics match those of previously reported Muse cells that were isolated from the BM and dermis [16,17,21], indicating that adipose tissue also contains Muse cells.

In adipose tissue, single-cell-derived cluster formation in suspension was unique to adipose-Muse cells; however, cluster formation ratio did not always reach 100% (Supplementary Table S1). This may be in part because of cellular damage caused by laser irradiation in the process of FACS isolation. Alternatively, cells might have been in an inactive dormant state, such that they did not proliferate. This property of Muse cells requires further study.

While MSCs are known to provide trophic and anti-inflammatory effects, these effects are temporary and do not